NASA Contractor Report 4090

A Study of the Effects of Reynolds Number and Mach Number on Constant Pressure Coefficient Jump for Shock-Induced Trailing-Edge Separation

Atlee M. Cunningham, Jr.,
and Gregory S. Spragle

CONTRACT NAS1-17955
AUGUST 1987

NASA

NASA Contractor Report 4090

A Study of the Effects of Reynolds Number and Mach Number on Constant Pressure Coefficient Jump for Shock-Induced Trailing-Edge Separation

Atlee M. Cunningham, Jr.,
and Gregory S. Spragle
General Dynamics Corporation
Fort Worth, Texas

Prepared for
Langley Research Center
under Contract NAS1-17955

National Aeronautics
and Space Administration

**Scientific and Technical
Information Office**

1987

A STUDY OF THE EFFECTS OF REYNOLDS NUMBER AND MACH NUMBER ON CONSTANT PRESSURE COEFFICIENT JUMP FOR SHOCK-INDUCED TRAILING-EDGE SEPARATION

By

Atlee M. Cunningham, Jr., and Gregory S. Spragle

SUMMARY

A study was conducted to address the influence of Mach and Reynolds numbers as well as airfoil and planform geometry on the phenomenon of constant shock jump pressure coefficient for conditions of shock-induced trailing-edge separation (SITES). It was demonstrated that the phenomenon does exist for a wide variety of two- and three-dimensional flow cases and that the influence of free stream Mach number was not significant. The influence of Reynolds number was found to be important but was not strong. Airfoil and planform geometric characteristics were found to be very important where the C_p jump was shown to vary with the sum of (1) airfoil curvature at the upper surface crest and (2) camber surface slope at the trailing edge. It was also determined that the onset of SITES could be defined as a function of airfoil geometric parameters and Mach number normal to the leading edge. This onset prediction was shown to predict the angle of onset to within $\pm 1^{\circ}$ accuracy or better for about 90% of the cases studied.

INTRODUCTION

The phenomena of shock boundary-layer interaction and shock-induced separation as well as their influences on aircraft performance have been the subjects of intense research of many years. Shockless and other airfoil design techniques have minimized the adverse effects of these phenomena on transonic cruise vehicles. However, fighter aircraft which maneuver at transonic speeds frequently encounter extensive shock-induced separations due to the high incidence required to achieve high normal force. Optimum maneuver capability, which is of upmost importance to fighter aircraft survivability, is currently developed on the basis of limited experimental studies. Such design techniques are expensive and time consuming. More importantly, true optimum designs are most likely never realized because of the designers limited visibility and configuration inflexibility. Therefore, expansion of the design data base with theoretical or semi-empirical analysis and design methods is needed in order to achieve more optimum designs.

Development of analytical methods for treating shock-induced separation requires a basic understanding of the phenomenon. Pearcey provided a very illuminating discussion of the process for turbulent boundary layers in transonic flow over airfoils in Reference 1. His criteria for onset of shock-induced separation stated that it would occur when the shock pressure ratio reached 1.4 and the downstream pressure reached sonic value. However, he did not address the nearly constant pressure-rise amplitude through the shock once separation reached the airfoil trailing edge. Cunningham (Reference 2), found that if this pressure rise on the airfoil surface was cast as a pressure coefficient jump, $\langle C_p \rangle$, a nearly constant value resulted regardless of the upstream shock Mach number, angle of attack, or span station

location for finite wings. The value of $\langle C_p \rangle$ was found to vary from 0.44 to about 0.67 with Reynolds number for the limited cases examined. Thus, it appeared that, depending on how energetic the boundary layer was, only a given amount of the free-stream dynamic pressure would be recovered across a shock terminating on that boundary layer. The boundary layer would thicken aft of the shock to form the wedge angle necessary to satisfy the oblique shock relations as pointed out by Pearcey. The free surface defined by the thickened boundary layer was therefore perceived to couple with the lower surface flow in a universal manner analogous to the Kutta condition for attached flow, such that the limit value of $\langle C_p \rangle$ was maintained.

As a result of the above findings, the study summarized in this report was conducted to determine the effects of Reynolds number and Mach number on the value of $\langle C_p \rangle$ for shock induced trailing edge separation. The study addressed the influence of airfoil geometry on these effects in two-dimensional flows as well as planform geometry for three-dimensional flows. The first task was to develop an appropriate data base from published or other available sources of wind tunnel data with Reynolds and Mach number variation sufficient to establish constant $\langle C_p \rangle$ trends with Mach number, Reynolds number, and the geometric parameters. The next task involved processing the experimental data into the "shifted C_p plot" format from which the $\langle C_p \rangle$ values were determined. Finally, the results were analyzed to establish appropriate parameters that might be used by the designer or analyst to establish constant $\langle C_p \rangle$ values for a new aircraft design as well as conditions under which the phenomenon might occur. These results will also be helpful in evaluating wind tunnel test results and how they might be altered under full scale conditions.

SYMBOLS

A_{ted}	Non-dimensional parameter for indicating the transition to shock induced trailing edge separation (Equation 3)
b	Wing span, in
c	Wing or airfoil chord, in
C_p	Pressure coefficient $(p - p_\infty)/q$
C_p^*	Value of C_p for sonic velocity
C_{p1}, C_{p2}	Pressure coefficient value just forward and aft of the shock respectively
$\langle C_p \rangle$	Shock jump C_p value, $C_{p2} - C_{p1}$
$\langle C_p \rangle^*$	Reduced $\langle C_p \rangle$ for airfoil geometry effects (Equation 2)
$K'_{t\alpha}$	Transonic similarity parameter modified to account for airfoil incidence (Equation 1)
M	Mach number
M_∞	Free stream Mach number
M_n	Mach number normal to the leading edge, $M_\infty (\text{Cos } \Lambda_{le})$
MAC	Mean Aerodynamic Chord, in
p	Local static pressure, psi

p_∞	Free stream static pressure, psi
q	Free stream dynamic pressure, psi
c/R	Airfoil curvature at the upper surface crest non-dimensionalized by local wing chord
R_e	Reynolds number based on wing chord for two-dimensional flow and MAC for three-dimensional flow
t	Wing or airfoil thickness, in
x	Chordwise coordinate, in
y	Spanwise coordinate, in
$(x/c)_{crest}$	Chordwise location of the upper surface crest
$(1-x/c)_{crest}$	Chordwise location of the upper surface crest relative to the trailing edge
α	Angle of attack, positive nose up, deg.*
α_t	Wing twist angle, measured at the 2/3 span station, deg.*
α_{ted}	Angle of attack at which the trailing edge pressure diverges and switches from positive to negative signaling the onset of shock induced trailing edge separation, deg.*

* Angles are defined in degrees except in equations 1, 2 and 3 where they are defined in radians.

α_{err}	$\alpha ted_{meas} - \alpha ted_{pred}$, deg.*
δ	One half airfoil thickness ratio, (t/2c)
$\delta_{lef}, \delta_{tef}$	Deflection of leading and trailing edge flaps, degrees (positive nose/trailing edge down), deg.*
δ_{tec}, DELTEC	Slope of the airfoil camber surface at the trailing edge (positive trailing edge down), deg.*
δ_{tel}, DELTEL	Slope of the lower airfoil surface at the trailing edge (positive trailing edge down), deg.*
γ	Ratio of specific heats, 1.4 for air and nitrogen
Λ_{le}	Leading edge sweep angle, deg.
η	Span station as a fraction of wing semi-span, y/(b/2)

* Angles are defined in degrees except in equations 1, 2 and 3 where they are defined in radians.

BACKGROUND

The development of shock-induced separation that extends to the trailing edge is a continuous process that can be separated into distinct phases, as discussed by Pearcey in Reference 1. These phases can be described as (1) the initial phase, where the shock is weak and the separated region is small and confined to the foot of the shock; (2) the transition phase, where the separation bubble grows rapidly until reaching the trailing edge; and (3) the final phase, where the trailing edge remains separated.

The pressure data shown in Figure 1 on a supercritical airfoil in two-dimensional flow (Reference 3) is a good example of typical pressure distributions that occur in the vicinity of the shock interacting with a separated turbulent boundary layer during the first phase. At $= 0.71^{\circ}$, 1.18°, and 1.567°, it will be noticed that the pressure coefficient just aft of the shock where the curves break (x/c~0.62-0.65) is about C_p*, which is the sonic value of C_p. Instead of trying to follow Rankine-Hugoniot conditions across the shock for increasing α, the velocity is remaining constant at the sonic value.

Schlieren photographs of typical shock/boundary-layer interactions, where the boundary layer is turbulent and separates at the shock, show that the shock is not normal to the airfoil surface. Comparing the shock angles and the "wedge" angles produced by separated boundary layers, the numbers are typical of supersonic wedge flows with oblique shocks where M = 1.0 is produced behind the shock. For example, for an upstream Mach number of 1.126, γ = 1.4, and a wedge angle of 2°, the shock angle is 18° from the normal and the Mach number aft of the shock is 0.9949 (Reference 4). As another example, for a wedge angle of 6° and an upstream Mach number of 1.285, the shock is inclined 24° from the normal

and the downstream Mach number is 0.9915.

Considering these observations and the fact that the flow is subsonic in the boundary layer, it makes sense that the local flow in the vicinity of the shock/wall intersection can adjust itself in response to a flow disturbance in order to maintain a velocity slightly less than sonic just aft of the shock. The maintenance of near sonic velocity is logical since it is the highest subsonic velocity that will permit forward propagation of disturbances. Thus we are led to the conclusion that an appropriate boundary condition to be satisfied across a shock on the wing surface is the maintenance of constant C_p (or velocity) aft of the shock if the boundary layer is turbulent and locally separated. This condition was incorporated in the transonic perturbation method (Reference 2) and was found to provide excellent agreement between theory and experiment for weak shocks on finite wings.

The transition phase usually occurs very rapidly according to Pearcey for two-dimensional flows and has been observed to do the same for three-dimensional flows. On finite wings, the spanwise spreading of shock-induced trailing-edge separation is the mechanism by which the transition seems to occur at a given span station as shown in Reference 3 for the ONERA M-6 wing at M = 0.92.

When the shock-induced separation reaches the trailing edge in the final phase, the shock-jump conditions change to another form of limiting condition. One well-known signal of this occurrence is trailing-edge pressure divergence in which the pressure coefficient at the trailing edge drops significantly from a positive value to a negative value for a small increase in α. This is illustrated in Figures 2 and 3 for η = 0.90 and Figures 3 and 4 for η = 0.65. Note also in these distributions that the character of the pressure

variation aft of the shock has changed. More importantly, the pressure rise across the shock, $\langle C_p \rangle$, is about constant for $\alpha = 4^o$ and 6^o at $\eta = 0.90$ and $\alpha = 6^o$ at $\eta = 0.65$.

This characteristic is highlighted in Figure 5 where the C_p distributions for several span stations and angles are plotted together in such a manner as to show the constant $\langle C_p \rangle$ at the shock. The circled symbols near the origin indicate how the origin of each plot was shifted relative to the distribution, $\alpha = 6^o$, $\eta = 0.65$, so as to superimpose the shock jump distribution. The fact that the origin shift is at an approximately constant C_p for a constant α indicates that C_{p1} and C_{p2} are constant along the span in the separated region. (The format shown in Figure 5 will be referred to as "shifted C_p plots" throughout this report).

In addition to $\langle C_p \rangle$ being constant for various α values and η stations, the C_p distributions just aft of the shock for some distance are also similar. Thus, the shock-induced flow-separation mechanism along the span must be the same with it beginning at the wing tip and progressing inboard. Since this mechanism involves flow separation, it was expected to be sensitive to Reynold's number.

Shown in Figure 6 is a plot similar to that shown in Figure 5 but for a C-141 model at various angles of attack. Although these data are all at a single span station, the angle of attack varies from 1^o to 4^o. The shock characteristics are similar to those shown in Figure 5 except for the $\langle C_p \rangle$ magnitude and the C_p distribution aft of the shock. The ONERA M-6 wing data in Figure 5 were obtained for a Reynold number based on the MAC of 11.7×10^6, and $\langle C_p \rangle$ is seen to be about 0.44. The C-141 data were obtained for $Re = 20 \times 10^6$ and the $\langle C_p \rangle$ is about 0.57. Figure 7 shows a limited set of data from C-5A flight test at two angles where again the characteristics are similar except that the $\langle C_p \rangle$ is

about 0.62 corresponding to $R_e = 80 \times 10^6$. Thus there seemed to be an increase in $\langle C_p \rangle$ with increasing Reynolds number. This corresponds to the ability of an increasingly energetic boundary layer to withstand an increasing shock pressure jump before separation.

Conditions under which the shock-induced trailing-edge separation occur, are expected to be a function of M_∞, α and airfoil characteristics. It was proposed in Reference 2, that a relationship based on the well-known transonic similarity parameter for thickness could be used to account for α as well. Evaluation of this equation for determining when shock-induced trailing-edge separation covered the outer 30% of the span led to inconclusive results. However, some modification yielded a form that did seem to be more universal, as is given in the following expression:

$$K'_{t\alpha} = \frac{M_\infty^2}{2} \frac{\sqrt{1 - M_\infty^2}}{\left[\frac{\gamma+1}{2}(\alpha + \delta)\right]^{2/3}} \qquad (1)$$

where δ is one half of the wing thickness ratio and $\gamma = 1.4$ for air. Examples of application of the above equation to various cases in the data base of Reference 2 are tabulated below:

	t/2c (at $\eta = 0.70$)	M_∞	α_{ted}	$K'_{t\alpha}$
Convair 880	0.0424	0.80	8.7°(-)	0.507
		0.85	8.8°(-)	0.499
		0.89	8.7°(-)	0.477
Onera M-6 Wing	0.0500	0.88	6.0°(+)	0.565
		0.92	5.0°(-)	0.552
F-111 TACT	0.0357	0.854	10.2°(-)	0.470
		0.901	8.2°(-)	0.491

The (-) or (+) α_{ted} notation indicates whether separation had already occurred (-) at some lower angle or was about to occur at a slightly higher angle (+). It appears that $K'_{t\alpha} < 0.55$ indicates that the outer third of the wing should be separated. However, if the outer 15% of the wing is to be used as the indicator to trigger application of the trailing-edge separation model, a higher value of $K'_{t\alpha}$ would be necessary.

This background forms the basis for a more extensive investigation of the constant $\langle C_p \rangle$ phenomenon for shock induced trailing edge separation (SITES). The first step will be to develop an appropriate data base using existing experimental data from tests in which SITES occurred. Two and three dimensional data for both conventional and supercritical airfoils are desired in order to establish the correct trends with Reynolds number, Mach number and geometry.

DATABASE DEVELOPMENT

The data used for refinement of the characteristics of the constant $\langle C_p \rangle$ concept were obtained from existing sources for the purpose of this study. Reference 3 contained a wealth of relevant two-dimensional as well as other three-dimensional data besides the ONERA M-6 wing results. Another vast source of information resided in both published and unpublished data from NASA Langley and Ames. General Dynamics has also published a significant data base as Volumes III through VII of Reference 2. Data for the C-141 and C-5 are available in reports published by Lockheed for both NASA and the Air Force.

Data Requirements

The requirements necessary for the data to be relevant to this study are quite specific. The increment of incidence change must be on the order of 1^{o} but not more than 2^{o}, so that experimental perturbations are not "smeared" by excessive shock motion. The range of maximum incidence must be such that several data points are available after the initial appearance of trailing-edge separation at some point on the wing. Reynolds and Mach number variations are desired for a given configuration. Most importantly, the spacing of pressure orifices must be close enough to accurately identify the shock pressure-rise characteristics and the shock location.

In order to isolate airfoil effects from those due to planform geometry, two-dimensional data are needed with sufficient Mach and Reynolds number variation for a fixed airfoil shape. Three-dimensional data are needed to establish planform effects and to distinguish essential differences between two- and three dimensional flows. Finally, other data from which the occurrence of shock induced trailing edge separation can be identified can be used to further refine the definition of onset conditions. These last data sets do not have to meet the above requirements for determining $<C_p>$ values, but only need to contain information relevant to trailing edge pressure coefficient divergence.

Two-Dimensional Data

The two-dimensional data used in this study were obtained from References 3 and 6 through 9 and data which is as yet unpublished on the NACA 0012 airfoil. This data was obtained from the Langley 0.3-meter Transonic Cryogenic Tunnel (0.3-m TCT) by C. L. Ladson. Examples of other data

sources considered but not used because of their failure to meet the above requirements are listed as References 10 through 13. Table 1 summarizes the data sets used to define the constant $<C_p>$ characteristics for SITES flows over various airfoils. Airfoil types, Mach and Reynolds number ranges and wind tunnel test facilities are listed for easy reference. Unfortunately, most of the data as well as all of the high R_e data were obtained in the NASA 0.3-m TCT so that it was difficult to determine if wind tunnel characteristics were important. The availability of data pertinent to this study was limited since SITES occurs at conditions which are significantly off-design and are thus of little interest in airfoil design development.

The MBB-A3 and ONERA D airfoils listed in Table 1 were chosen specifically because data are also available for three-dimensional configurations which use these airfoils. Hence, these data are helpful in separating two and three-dimensional flow effects.

Three-Dimensional Data

The three-dimensional data used in this study were obtained from References 3, 5, 14, 15 and 16. Table 2 summarizes the data sets used to define the constant $<C_p>$ characteristics for SITES flows over various configurations. As mentioned above, two configurations had airfoil sections which were included in the two-dimensional data sets. The ONERA M-6 wing used the ONERA D airfoil section and the MBB wing/body used the MBB-A3 airfoil section.

Most of the applicable data available were obtained from wind tunnel tests, however, C-141 and C-5A data were also available from flight test. This extended the Reynolds number range to 80×10^6 with intermediate points at 20, 45 and 58×10^6. The F-16 pressure model data, ref. 15, also included

various leading edge flap deflections. Aspect ratios varied from 3 for the F-16 to about 8 for the C-141 and C-5A. Wing sweeps varied from about 27^{o} for the C-141 and C-5A to 40^{o} for the F-16. Test facilities were different for all configurations which included five wind tunnels as well as flight test.

Data for Onset Determination

These data sets were used to further establish what conditions were necessary for the occurrence of SITES. Since only one or two incidences were needed, one prior to and the other after SITES, many of the cases available in the two- and three- dimensional data bases which did not qualify for determining $\langle C_p \rangle$, would qualify for onset determination. In addition, the pressure data for the F-111 TACT model given in Reference 2 (Vol. IV), provided onset information for a different configuration with a supercritical airfoil section.

DATA PROCESSING

Data processing was accomplished in four steps: (1) reviewing existing plots and/or tabulated data sets to select appropriate data for analysis; (2) replotting all data in a consistent format; (3) producing the shifted C_p plots; and (4) determining $\langle C_p \rangle$ values. In order to facilitate the investigation, an existing plotting program was modified for the purposes of this study. The plot program was coded for the General Dynamics/Fort Worth VAX computer system with an input format which eliminated redundant input for multiple pressure data sets. The capability was also developed to permit shifting of pressure data sets to align shock location; this was done by hand in prior investigations, see ref. 2. Finally, a technique was incorporated in the program to calculate $\langle C_p \rangle$ values in a consistent manner through the

use of least squares fits of the shifted C_p plot data.

This section will present a description of the data processing for producing the shifted C_p plots and determining $\langle C_p \rangle$ values using the least squares technique.

Shifted C_p Plots

A sample of the final shifted C_p plot format is shown in Figure 8. This sample shows three pressure data sets for α = 1.5°, 2.0° and 3.0° where data for the two higher α sets were shifted so as to match the shock jump characteristics with the data at α = 1.5°. The plot ordinate and absissa are shown for the α = 1.5° data set which is referred to as the "REF" data as denoted on the plot. The sonic value, C^*_p, is also denoted for the "REF" data. Origin shifts for the higher α data are denoted as circled symbols for each of the data sets. An aft shift means that the shock has moved forward and a downward shift means that C_p just upstream of the shock, has become more negative.

A complete set of the shifted C_p plots is available in the Appendix. An index of these plots is given in Table 3 according to configuration, Mach and Reynolds numbers and figure numbers.

Estimation of $\langle C_p \rangle$

A technique was formulated for automatically calculating $\langle C_p \rangle$ values in a consistent manner. The technique makes use of local least squares curve fits in three user selected regions of the shifted C_p plots as shown in Figure 9. The three regions, upstream, shock and downstream, are determined as approximate bounds by the user by specifying the appropriate x/c values. Curve fits of up to quartic in x/c are used in each of the regions to define mean curves as

illustrated in Figure 9. The two intersections with the shock fit curve then become the shock C_p values from which $\langle C_p \rangle$ is determined. A shock C_p slope is also defined as $\langle C_p \rangle / \Delta x$ where Δx is the "width" of the shock rise as defined by the curve intersections. It is not necessary for the curve intersections to correspond with the region boundaries; however, they were usually quite close to each other.

A sample plot produced with this technique is shown in Figure 10. The plot format is expanded for higher resolution to include only the x/c limits specified by the user. Data listed in the table in Figure 10 show the $\langle C_p \rangle$, $\langle C_p \rangle / \Delta x$, and the corresponding curve fit order for each region (1 means linear fit, 2 means parabolic, etc.). Curve fits up to fourth order could be used in each region. The regions are numbered sequentially, 1, 2 and 3 corresponding to upstream, shock, and downstream respectively. As shown in this example, several combinations of curve fits are used to evaluate stability of the fit. In this case, a 3, 2, 3 (cubic, parabolic, cubic) fit was selected, however later analysis of all data showed that 2, 1, 2 (parabolic, linear, parabolic) produced more consistent results. In some cases where insufficient data points were available for determining a reasonable fit, the $\langle C_p \rangle$ values were read by hand as done in the early investigations.

RESULTS AND ANALYSIS

Results for the variation of $\langle C_p \rangle$ with Mach and Reynolds number were obtained for both two and three-dimensional flows. Mach and Reynolds number effects as well as airfoil geometric influences were separated for two-dimensional flows. Wing geometry effects were then determined for three-dimensional flows which included both wind tunnel and flight test data. The onset of shock induced trailing edge

separation was determined for all cases considered and was cast in the form of a non-dimensional parameter.

This section will present the two- and three-dimensional flow results for $\langle C_p \rangle$ variations with various quantities as well as results for the onset parameter study.

Two-Dimensional Constant $\langle C_p \rangle$ Characteristics

The two-dimensional $\langle C_p \rangle$ data generated in this study are tabulated in Table 4 and the pertinent airfoil geometry data are given in Table 5. Variation of $\langle C_p \rangle$ with Mach number is shown in Figure 11. With exception of the data for the ONERA "D" airfoil and the NACA 0012 airfoil at M=0.82, all data are bounded between a $\langle C_p \rangle$ of approximately 0.5 and 0.6. These results imply that there is no conclusive trend with free stream Mach number. This is not too surprising, however, since the value of $\langle C_p \rangle$ seems to be relatively independent of the upstream Mach number for both two- and three-dimensional flows.

The variation of $\langle C_p \rangle$ with free-stream Reynolds number (based on the airfoil chord) is shown in Figure 12. These results show a trend of increasing value with R_e, however, the data spread makes it difficult to determine the exact trend. The spread in data at R_e = 15 and 30 x 10^6 for the NACA 0012 and SC(3) airfoils was used to analyze the effects of airfoil parameters since these airfoils were significantly different. The results of this study are shown in Figure 13 where the parameter

$$\langle C_p \rangle^* = \frac{\langle C_p \rangle}{[\, c/R + \delta_{tec} \,]^{2/3}} \qquad (2)$$

is plotted against R_e. The basis for this parameter lies in the non-dimensional transonic similarity parameter, Eqn. 1, which was discussed earlier. Inclusion of Mach number in the parameter was not successful, as might be expected based on the trends shown in Figure 11. The most remarkable results shown in Figure 13 are the reduction of scatter at R_e = 15 and 30 x 10^6 and the lining up of these points with the R-4 airfoil data at R_e = 40 x 10^6.

In order to reduce scatter at constant Reynolds number, the values of $\langle C_p \rangle$ at different Mach numbers but constant Reynolds number were averaged together. Replotting this "averaged" two-dimensional data in the same formats as in Figures 12 and 13, yields more clearly defined trends as shown in Figures 14 and 15. Figure 14 allows the separation of airfoil effects where as Figure 15 emphasises the collapsing of the data to a more orderly variation with R_e. A possible trend which could be suggested from Figure 15 is a reduction of data scatter with increasing R_e, as indicated by the dashed envelope. The limit to which the data appear to converge at higher R_e seems to be constant at about 0.88 which also lines up with several points at lower values of R_e that include NACA 0012, SC(3) and CAST 10 airfoil data.

Figures 14 and 15 also show some added data points for two different symmetrical bi-convex airfoils at zero angle-of-attack. These data were obtained from Reference 17 for a 12% thick bi-convex airfoil and from Reference 18 for an 18% thick bi-convex airfoil. In both cases, the shock-induced separation was reached through an increase in Mach number instead of an increase in α. The $\langle C_p \rangle$ values for the bi-convex airfoils in Figure 14 agree very well with each other, however, the $\langle C_p \rangle^*$ values in Figure 15 do not. Since the bi-convex airfoils at zero incidence have symmetric separated flows, it is quite probable that they cannot be classified in the same way as the non-symmetrical cases.

This, however, raises a fundamental question as to how would the flow transition from symmetric to unsymmetric when SITES already exists on a symmetric airfoil at zero incidence and the incidence is increased. According to the observations, incidence is supposed to have little influence on the value of $<C_p>$ once SITES has occurred.

Another point that needs to be made about the data shown in Figures 11 through 15 is that many of the tests were conducted in the NASA Langley 0.3-m TCT. As shown in Table 1, data for the NACA 0012, SC(3), CAST 10 and DFVLR R-4 airfoils were obtained in that facility. Noting the spread of these data as well as those from other facilities, however, it appears that the data source has no particular influence on the grouping of results.

The reason for the $<C_p>$ scatter at lower R_e values and the reduction in scatter at higher R_e is attributed to the influence of the location of transition from laminar to turbulent boundary layer. With larger distances between the stagnation point and the transition point at lower R_e values, the effects of tunnel turbulence and other sources of unsteadiness would have a greater impact on where the boundary layer would actually transition. Thus, a more aft transition point would seem to lead to a greater uncertainty in the boundary layer development. This hypothesis is somewhat justified on the basis of lower scatter in the data obtained for the SC(3) airfoil with fixed transition. These data are denoted as the solid square symbols in Figure 15.

In summary, the two-dimensional results show that the average value of $<C_p>$ for SITES tends to increase as the sum of (1) airfoil curvature at the upper surface crest and (2) trailing edge camber line slope. In this relationship, the airfoil curvature is expressed as the reciprocal of the radius of curvature non-dimensionalized by the wing chord.

Data scatter is present at low Reynolds number values but essentially disappears by about R=30x10^6 based on the wing chord. Above R_e = 30x10^6, there seems to be little effect due to Reynolds number up to 40x10^6. No data were available above R_e = 40x10^6, hence the trend could not be verified beyond this point. A question was also raised on how symmetric SITES may differ from unsymmetric SITES and how does the flow transition from symmetric to unsymmetric.

Three-Dimensional Constant $\langle C_p \rangle$ Characteristics

The $\langle C_p \rangle$ data generated in this study for all three-dimensional flow cases are tabulated in Table 6 along with pertinent configuration geometry data in Table 7. Variation of $\langle C_p \rangle$ with Reynolds number (based on wing MAC) is shown in Figure 16. Because flight test data for the C-141 and C-5A aircraft are included, the Reynolds number range was extended to 80x10^6. The same data are replotted as $\langle C_p \rangle^*$ in Figure 17 which also indicate a trend toward less scatter for R_e>30x10^6. Collapsing of the $\langle C_p \rangle$ data in Figure 16 to the $\langle C_p \rangle^*$ data in Figure 17 is quite convincing evidence of the airfoil parameter influence. An average of the C-141 and C-5A $\langle C_p \rangle^*$ data for R_e>20x10^6 was found to be 1.013, shown in Figure 17 as a dashed line, where all of these data points fall very close to the line with exception of the C-141 point at R_e = 58x10^6.

The airfoil parameters given in Table 7 were determined at about 2/3 span of the wing. Although some of the wings were twisted, only the airfoil parameters were used. When the data for two-dimensional flow in Figure 15 are compared with the three-dimensional data in Figure 17, the values of $\langle C_p \rangle^*$ appear to be in the same range. Because of the differences in two- and three-dimensional flows, it was initially believed that the two would be incompatible. However, combining these data produces the plot shown in

Figure 18 in which it is apparent that the data are compatible. All three-dimensional data for $R_e<15x10^6$ fit within the scatter boundary developed for two-dimensional flow. Data for the C-141 and C-5A at higher values of R_e all tend to fall along a constant line as shown in Figure 17. This characteristic is similar to the two-dimensional characteristic that suggested $<C_p>^*$ would be independent of R_e for $R_e>30x10^6$.

It is apparent in Figure 18 that a conflict exists with regard to geometry and three-dimensional effects. The data for $R_e<15x10^6$ are limited to the ONERA M-6 wing, F-16 1/9-scale model and the MBB wing/body configurations in addition to two values for a C-5A model. Since these data fall within the scatter boundary defined by two-dimensional flow, the source of the conflict is the fact that the "constant" trends defined at higher R_e for both two- and three-dimensional flow do not agree. The constant trend for three-dimensional flow is mostly defined by C-141 flight test data with a single point at $R_e = 80x10^6$ from C-5A flight test.

The determination of geometric parameters for the C-141 that were used to calculate $<C_p>^*$ is believed to be a potential source of this disagreement. The values of c/R and δ_{tec} were calculated based on interpretation of the airfoil description given in Reference 19 rather than actual airfoil ordinates as was possible for the other configurations. For example, if the sum of c/R and δ_{tec} estimate for the C-141 was increased by 10%, the constant value, $<C_p>^*=1.013$, would be lowered to about 0.95. A geometric error for the C-141 would only affect the absolute value of the data trend and would not change the trend itself since all values would be divided by the same constant.

The C-5A $\langle C_p \rangle^*$ value at $R_e = 80 \times 10^6$ is not subject to the uncertainty associated with the C-141 data; thus, a weak increase of $\langle C_p \rangle^*$ with R_e is indicated by the results shown in Figure 18. Earlier investigations of this phenomenon discussed in Reference 2 considered the possible increase of $\langle C_p \rangle$ with $R_e^{1/5}$ which was based on the variation of a turbulent boundary layer thickness. Hence, dividing $\langle C_p \rangle^*$ by $R_e^{1/5}$ should produce a constant trend at high R_e. A plot of this function for the data in Figure 18 is shown in Figure 19. The C-141 data do not show a constant trend, however, the C-5A value at 80×10^6 and the R-4 value at 40×10^6 are nearly equal. Again, for $R_e > 20 \times 10^6$, the C-141 data seem to be displaced which if lowered would tend to fall in line with the other high R_e data. The rise of $\langle C_p \rangle^* / R_e^{1/5}$ for $R_e < 30 \times 10^6$ is due to the trend that $\langle C_p \rangle^*$ is centered about a constant value of 0.88 which, when divided by $R_e^{1/5}$ tends to infinity as R_e goes to zero.

Onset of Shock Induced Trailing Edge Separation

The onset of conditions under which the constant $\langle C_p \rangle$ phenomenon exists also coincides with the divergence of trailing edge pressures. This trailing edge divergence, where the pressure coefficient becomes negative signaling loss of pressure recovery, is a well know indicator of buffet onset. Identification of the onset is of upmost importance for design information and represents a significant part of this research program.

The results of the onset study are shown in Figure 20 where the parameter

$$A_{ted} = \frac{M_n \sqrt{1 - M_n^2} \left[\left(1 - x/c \right)_{crest} \left(c/R + \delta_{tel} \right) \right]^{1/3}}{2 \left[\frac{1+\gamma}{2} \left(c/R + \frac{a_{ted} + a_t + 0.8\,\delta_{tec}}{\left(1 - x/c \right)_{crest}} \right) \right]^{2/3}} \qquad (3)$$

is plotted as a function of Reynolds number for all two- and

three-dimensional data. This quantity is also based on the transonic similarity term, K'_{ta}, with several modifications which were determined through an extensive parameter study. For two-dimensional flow, the wing twist angle, α_t, is naturally zero but in three-dimensional flow, it is taken at the 2/3 span station where other airfoil geometric data are determined. The onset study results are tabulated in Tables 8 and 9 for two- and three-dimensional data respectively.

The data shown in Figure 20 represent three possibilities: (1) before SITES (open symbols), (2) at SITES (half-filled symbols) and (3) after SITES (solid symbols). Three-dimensional data are denoted by flagged symbols at which onset is considered to occur when the outer 1/3 of the wing is in SITES flow. These results show that the transition to SITES is indicated approximately by a mean value, $A_{ted} = 0.19$, where below that value the constant $\langle C_p \rangle$ phenomenon should occur. Generally, the spread of transition points about the mean value of 0.19 is within the $\pm$5% bounds (ie. 0.18 to 0.20) with only two points lying outside these bounds. There does not appear to be a clearly defined trend with Reynolds number except that the average A_{ted} might be slightly higher at about 0.195 as $Re \rightarrow 0$.

The use of Mach number normal to the leading edge for three-dimensional data,

$$M_n = M_\infty \cos \Lambda_{le}$$

was found to provide the best correlation of results. The average of leading edge and trailing edge sweep angles was also considered, however, since most of the wings had nearly the same sweep for both leading and trailing edges, this variation was not significant. The F-16, with $\Lambda_{le} = 40^\circ$ and $\Lambda_{te} = 0^\circ$ did show a considerable sensitivity to this effect and hence was the deciding factor in selecting the leading

edge sweep for determining M_n.

The validity of using $A_{ted} = 0.19$ as an indicator for signaling transition to SITES was evaluated by comparing α_{ted} values calculated from $A_{ted} = 0.19$ with actual measured values. These data are also listed in Tables 8 and 9 and plotted in Figure 21. The solid line shown in Figure 21 represents perfect correlation whereas the dashed lines represent a difference of $\pm 1^{\circ}$ between measured and predicted α_{ted} values. The distribution of measured transition points relative to the $\pm 1^{\circ}$ error band, which represents a reasonable accuracy, is listed below:

Error Band	No. of Transition Points
$\alpha_{err} > 1.0^{\circ}$	2
$-1.0^{\circ} \leq \alpha_{err} \leq 1.0^{\circ}$	18
$\alpha_{err} < -1.0^{\circ}$	1

where

$$\alpha_{err} = \alpha ted_{meas} - \alpha ted_{pred}$$

For conditions prior to transition the distribution is

Error Band	No. of Pre-Transition Points
$(\alpha_{meas} - \alpha ted_{pred}) > 1.0^{\circ}$	1
$(\alpha_{meas} - \alpha ted_{pred}) \leq 1.0^{\circ}$	12

and for conditions after transition the distribution is

Error Band	No. of Post-Transition Points
$(\alpha_{meas} - \alpha ted_{pred}) \geq -1.0$	15
$(\alpha_{meas} - \alpha ted_{pred}) < -1.0$	1

These results provide an evaluation of the accuracy of the prediction method on a statistical basis assuming an error of $\pm 1.0^{\circ}$, where the predictions for transition were accurate to within $\pm 1^{\circ}$ for 18 out of 21 samples. Flow had not transitioned for angles less than ($\alpha ted_{pred}+1^{\circ}$) for 12 out of 13 samples and it had already transitioned by ($\alpha ted_{pred}-1^{\circ}$) for 15 out of 16 samples.

The onset study has thus provided a parameter for predicting the onset of SITES for a fairly wide range of configurations and conditions. The accuracy of the predicted angle for transition is nominally $\pm 1^{\circ}$ although the accuracy is probably much better and nearer to $\pm 0.5^{\circ}$. The parameter, A_{ted}, is based only on airfoil and planform geometry information and the free-stream Mach number, thus for the cases studied, no information was needed from pressure distributions.

Influence of Control Surfaces

Since the constant $<C_p>$ phenomenon has been so closely tied to airfoil geometry in this study, one would expect it to be significantly influenced by the deflection of leading and/or trailing edge control surfaces. Considering the geometric parameters in either $<C_p>^*$ or A_{ted}, it would appear that a leading edge flap would not have any significant effect. This conclusion was verified with the F-16 data set where test conditions included leading edge flap settings of 0°, 5° and 10°. Data are shown in Figure 22 for δ_{lef}'s of 0°, 5° and 10° at M=0.9, in shifted C_p plot format. As can be seen, the deflected flap data fall right in with the undeflected data. This same result was obtained for the other Mach numbers and in no case could an influence on either $<C_p>$ amplitude or onset be defined.

With regard to trailing edge flap deflection, δ_{tef}, no data were available in the data base surveyed. Considering the importance of δ_{tec} and δ_{tel} in the $\langle C_p \rangle^*$ and A_{ted}, this is unfortunate since δ_{tef} would be added to both δ_{tec} and δ_{tel}. For a constant $\langle C_p \rangle^*$, trailing edge flap deflected down would lead to a higher value of $\langle C_p \rangle$. For a constant A_{ted}, the same downward flap deflection would lead to a lower value for α_{ted}. Remembering that δ_{tel} is in the numerator of A_{ted}, the influence on α_{ted} would not quite be as great as on $\langle C_p \rangle$.

The effect of leading and trailing edge control surface deflection would be another area for further investigation. The influence of Reynolds number could be more important where regions of high curvature exist in the vicinity of the hinge line. The control surface effect would also be influenced by the control deflection angle as well as both two- and three-dimensional flows. For the latter, the stabilizing effect of spanwise flow would be expected to be very important. Therefore a test program could be envisioned that included several airfoils plus leading and trailing edge flaps as well as a finite wing planform using at least one of these airfoils, all of which would be tested over a wide range of Reynolds number.

CONCLUSIONS AND RECOMMENDATIONS

A study was conducted to address the influence of Mach and Reynolds numbers as well as airfoil and planform geometry on the phenomenon of constant shock jump C_p, $\langle C_p \rangle$, for conditions of shock induced trailing edge separated (SITES) flows. It was demonstrated that the phenomenon does exist in a wide variety of two- and three-dimensional flow cases and that the influence of free stream Mach number was not significant. The influence of Reynolds number was found to be important in that for $R_e < 30 \times 10^6$ there was more scatter in

the $<C_p>$ results and for $R_e > 30 \times 10^6$ there seemed to be a trend for $<C_p>$ to be weakly dependent on R_e.

The effect of airfoil and planform geometry was found to be very important. It was shown that $<C_p>$ increased as the sum of (1) airfoil curvature at the upper surface crest and (2) camber line slope at the trailing edge was increased. It was also determined that the onset of shock induced trailing edge separation could be defined in both two- and three-dimensional flows as a function of airfoil geometric parameters and Mach number normal to the leading edge. The resulting prediction technique provided estimates of the onset within an error bounds of $\pm 1^\circ$ or better for about 90% of the cases studied.

As a result of the findings of this study, several recommendations are offered to answer some of the questions that have been raised. The two-dimensional characteristics have been shown to be strongly related to the three-dimensional characteristics, this enables airfoil tests to be conducted to provide a better understanding of three-dimensional flows. The recommendations are as follows:

1. It is recommended that a symmetric airfoil such as the NACA 0012 be re-tested starting with $\alpha = 0^\circ$ but with Mach numbers high enough to produce SITES. Once SITES is established, the incidence should be increased up to the point where the constant $<C_p>$ phenomenon disappears. This test has the objective of answering the question of how does a SITES flow transition from a symmetric to a non-symmetric flow and what happens to $<C_p>$ in the process.

2. A series of tests is recommended where all or some of the four basic airfoils, NACA 0012, SC(3), CAST 10 and

DFVLR R-4, be re-tested to a much higher Reynolds number, hopefully 80×10^6. This series of tests will have the objective of determining if the trend of increasing $\langle C_p \rangle^*$ with R_e for $R_e > 30 \times 10^6$ holds true for two-dimensional flows.

3. A third test is recommended where one of the above four airfoils is used on a finite wing with perhaps several leading edge sweeps of say 0°, 20° and 30°. This test will provide information on spanwise flow effects at higher Reynolds numbers than were available in the data base developed for the current study. If the NACA 0012 airfoil is used, this test could also include the investigation of transition from $\alpha = 0$, recommendation 1.

4. Finally, a series of test is recommended where leading and trailing edge flaps are investigated in two-dimensional flows. In addition, this should be extended to three-dimensional flow again using the NACA 0012 airfoil suggested in the first and third tests. The objective of this series of tests would be to identify the effect of flap deflection angles and Reynolds number interplay on the $\langle C_p \rangle^*$ and A_{ted} parameters.

REFERENCES

1. Pearcey, H. H.: Some Effects of Shock-Induced Separation of Turbulent Boundary Layers in Transonic Flow Past Aerofoils. Aeronautical Research Council Report R.& M. No. 3108, 1959.

2. Cunningham, A. M. Jr.; Sheridan, A. E.; and Freeman, T. K.: Update Structural Design Criteria, Design Procedures and Requirements for Bomber/Logistic Type Airplane Wing and Tail Loads. AFWAL-TR-82-3084, Volumes I through VII, December 1982.

3. AGARD: Experimental Data Base for Computer Program Assessment. AGARD-AR-138, May 1979.

4. Keenan, J. H. and Kaye, J.: Gas Tables. John Wiley & Sons, Inc., New York, 1957.

5. Cahill, J. F. and Connor, P. C.: Correlation of Data Related to Shock-Induced Trailing-Edge Separation and Extrapolation to Flight Reynolds Number. NASA CR-3178, September, 1979.

6. Johnson, W. G.,Jr.; Hill, A. S.; and Eichmann, O.: Pressure Distributions From High Reynolds Number Tests of a NASA SC(3)-0712(B) Airfoil in the Langley 0.3-Meter Transonic Cryogenic Tunnel. NASA TM-86370, July 1985.

7. Dress, D. A.; Stanewsky, E.; McGuire, P. D.; and Ray, E. J.: High Reynolds Number Tests of the CAST 10-2/DOA 2 Airfoil in the Langley 0.3-Meter Transonic Cryogenic Tunnel — Phase II. NASA TM-86273, August 1984.

8. Jenkins, R. V.; Johnson, W. G., Jr.; Hill, A. S.; Mueller, R.; and Redeker, G.: Data From Tests of a R4 Airfoil in the Langley 0.3-Meter Transonic Cryogenic Tunnel. NASA TM-85739, September 1984.

9. Bernard-Guelle, R.: Essais En Transsonique Du Profil D. Influence Du Nombre De Reynolds. ONERA Report No. 10/1685 AN, January 1972.

10. Harris, C. D.: Two Dimensional Aerodynamic Characteristics of the NACA 0012 Airfoil in the Langley 8-Foot Transonic Pressure Tunnel. NASA TM-81927, April 1981.

11. Johnson, W. G.,Jr.; Hill, A. S.; Ray, E. J.; Rozendaal, R. A.; and Butler, T. W.: High Reynolds Number Tests of a Boeing BAC I Airfoil in the Langley 0.3-Meter Transonic Cryogenic Tunnel. NASA TM-81922, April 1982.

12. Jenkins, R. V.: Reynolds Number Tests of an NPL 9510 Airfoil in the Langley 0.3-Meter Transonic Cryogenic Tunnel. NASA TM-85663, 1983.

13. Plentovich, E. B.; Ladson, C. L.; and Hill, A. S.: Tests of a NACA 65_1-213 Airfoil in the NASA Langley 0.3-Meter Transonic Cryogenic Tunnel. NASA TM-85732, February 1984.

14. Elbers, W. K.: Wind Tunnel Data Report 1/9-Scale F-16A Pressure Model Investigation of Shock-Induced Separation for Limit Cycle Oscillation Studies (AEDC PWT-16T Test TF-695). General Dynamics Fort Worth Division Report 16PR4694, September 1985, (Contract No. F33657-84-C-2034).

15. Cahill, J. F. and Cooper, B. L.: Flight Test Investigation of Transonic Shock-Boundary Layer Phenomena. AFFDL-TR-68-84, July 1968.

16. Flechner, S. G. and Patterson, J. C., Jr.: Tabulated Pressure Measurements on a Large Subsonic Transport Model Airplane with High-Bypass-Ratio, Powered, Fan-Jet Engines. NASA TM X-2530, May 1972.

17. Davis, S. and Satyanarayana, B.: Two-Dimensional Transonic Testing with Splitter Plates. NASA TP-1153, February 1978.

18. Rubesin, M. W.; Okuno, A. F.; Levy, L. L, Jr.; McDevitt, J. B.; and Seegmiller, H. L.: An Experimental and Computational Investigation of the Flow Field About a

Transonic Airfoil in Supercritical Flow With Turbulent Boundary-Layer Separation. NASA TM X-73157, July 1976.

19. MacWilkinson, D. G.; Blackerby, W. T.; and Paterson, J. H.: Correlation of Full-Scale Drag Predictions with Flight Measurements on the C-141A Aircraft — Phase II, Wind Tunnel Test, Analysis and Prediction Techniques. NASA CR-2333, 1974.

TABLE 1 - DATA SETS FOR TWO-DIMENSIONAL SITES FLOWS

AIRFOIL TYPE	MACH RANGE	REYNOLDS NO. RANGE	WIND TUNNEL	REFERENCE
NACA 0012 Conventional-Symmetric	0.76 - 0.82	$6 - 30 \times 10^6$	NASA 0.3-m TCT	unpublished
NASA SC(3)-0712(B) Supercritical	0.78 - 0.80	$10 - 30 \times 10^6$	NASA 0.3-m TCT	6
CAST-10-2/DOA Supercritical	0.78 - 0.80	$4 - 15 \times 10^6$	NASA 0.3-m TCT	7
DFVLR R-4 Supercritical	0.78	$4 - 40 \times 10^6$	NASA 0.3-m TCT	8
CAST 7 Supercritical	0.76	6×10^6	DFVLR - TWB	3
MBB - A3 Supercritical	0.76 - 0.85	6×10^6	ARA Bedford	3
ONERA D Shockless-Symmetric	0.81 - 0.85	4.5×10^6	ONERA R1-CH	9

TABLE 2 - DATA SETS FOR THREE-DIMENSIONAL SITES FLOW

CONFIGURATION	MACH RANGE	REYNOLDS NO. RANGE	WIND TUNNEL	REFERENCE
ONERA M-6 Wing Semi-Span Wing ONERA D Airfoil (Trans. Free)	0.88 - 0.93	12×10^6	ONERA S2MA	3
F-16 Model Complete A/C (Trans. Fixed)	0.90 - 0.93	2.5×10^6	AEDC PWT-16T	14
MBB Wing/Body Full Span Wing/Body MBB-A3 Airfoil (Trans. Free)	0.88 - 0.92	1.34×10^6	DFVLR 1x1 Meter Transonic Tunnel	3
C-141 Model Complete A/C (Trans. Free)	0.85	25×10^6	?	5
C-141 Aircraft Flight Test (Trans. Free)	0.84 - 0.85	$45 - 72 \times 10^6$	Flight Test	5
C-5A Model Wing/Body (Trans. Fixed)	0.775	8×10^6	LRC 8-Ft Transonic Tunnel	16
C - 5A Aircraft Flight Test (Trans. Free)	0.85	58×10^6	Flight Test	5

TABLE 3 - INDEX OF SHIFTED C_p PLOTS

CONFIGURATION	MACH	R_e	FIGURE
NACA 0012 Airfoil	0.76	$6x10^6$	A-1
"	0.80	"	A-2
"	0.82	"	A-3
"	0.74	$9x10^6$	A-4
"	0.76	$15x10^6$	A-5
"	0.78	"	A-6
"	0.80	"	A-7
"	0.74	$30x10^6$	A-8
SC(3)-0712(b)Airfoil	0.78	$10x10^6$	A-9
"	0.79	"	A-10
"	0.80	"	A-11
"	0.78	$15x10^6$	A-12
"	0.80	"	A-13
"	0.78	$30x10^6$	A-14
"	0.79	"	A-15
"	0.80	"	A-16
"	0.78*	$10x10^6$	A-17
"	0.78*	$15x10^6$	A-18
"	0.78*	$30x10^6$	A-19
CAST 10-2/DOA Airfoil	0.78	$4x10^6$	A-20
"	0.79	"	A-21
"	0.80	"	A-22
"	0.80	$6x10^6$	A-23
"	0.79	$10x10^6$	A-24
"	0.80	"	A-25
"	0.78	$15x10^6$	A-26
"	0.79	"	A-27
"	0.80	"	A-28

* Fixed Transition

TABLE 3 (cont'd)

CONFIGURATION	MACH	R_e	FIGURE
DFVLR R4 Airfoil	0.78	$4x10^6$	A-29
"	0.78	$15x10^6$	A-30
"	0.78	$40x10^6$	A-31
CAST 7 Airfoil	0.76	$6x10^6$	A-32
MBB-A3 Supercritical Airfoil	0.80	$6x10^6$	A-33
ONERA D Airfoil	0.81	$4.5x10^6$	A-34
"	0.84	"	A-35
ONERA M-6 Wing	0.88	$12x10^6$	A-36
"	0.93	$12x10^6$	A-37
F-16 1/9-Scale Model	0.90	$2.5x10^6$	A-38
"	0.91	"	A-39
"	0.92	"	A-40
"	0.93	"	A-41
MBB Wing/Body	0.90	$1.34x10^6$	A-42

TABLE 4. TABULATED C_p JUMP RESULTS FOR TWO-DIMENSIONAL AIRFOIL DATA

Airfoil	Mach	RexE06	Cp Jump	Cp Jump *	Cp Jump * / RE**.2	Slope	Terms
NACA—0012 (NASA 0.3-m TCT)	Ø.76ØØ	6.ØØØØ	Ø.51Ø5	Ø.8668	Ø.ØØ382	6.433Ø	3/1/3
	Ø.76ØØ	6.ØØØØ	Ø.4947	Ø.84ØØ	Ø.ØØ37Ø	9.758Ø	2/1/2
	Ø.8ØØØ	6.ØØØØ	Ø.5Ø15	Ø.8515	Ø.ØØ375	6.5ØØ2Ø	3/1/3
	Ø.8ØØØ	6.ØØØØ	Ø.5277	Ø.896Ø	Ø.ØØ395	6.5ØØ2Ø	2/1/2
	Ø.8ØØØ	6.ØØØØ	Ø.5269	Ø.8946	Ø.ØØ394	6.56ØØ	2/1/2
	Ø.82ØØ	6.ØØØØ	Ø.4483	Ø.7612	Ø.ØØ336	1Ø.76ØØ	3/2/3
	Ø.82ØØ	6.ØØØØ	Ø.4458	Ø.7569	Ø.ØØ334	11.242Ø	2/1/2
	Ø.74ØØ	9.ØØØØ	Ø.5487	Ø.9317	Ø.ØØ379	8.143Ø	2/2/2
	Ø.74ØØ	9.ØØØØ	Ø.5475	Ø.9296	Ø.ØØ378	8.312Ø	2/1/2
	Ø.74ØØ	9.ØØØØ	Ø.549Ø	Ø.9322	Ø.ØØ379	8.4Ø3Ø	2/1/2
	Ø.76ØØ	15.ØØØØ	Ø.5147	Ø.8739	Ø.ØØ321	5.819Ø	2/1/2
	Ø.76ØØ	15.ØØØØ	Ø.51ØØ	Ø.8659	Ø.ØØ318	7.18ØØ	READ*
	Ø.78ØØ	15.ØØØØ	Ø.4797	Ø.8145	Ø.ØØ299	6.616Ø	2/1/2
	Ø.78ØØ	15.ØØØØ	Ø.47ØØ	Ø.798Ø	Ø.ØØ293	5.819Ø	READ*
	Ø.8ØØØ	15.ØØØØ	Ø.49ØØ	Ø.832Ø	Ø.ØØ3Ø5	7.ØØØØ	READ*
	Ø.8ØØØ	15.ØØØØ	Ø.4964	Ø.8429	Ø.ØØ3Ø9	7.839Ø	1/1/1
	Ø.74ØØ	3Ø.ØØØØ	Ø.5183	Ø.88ØØ	Ø.ØØ281	9.524Ø	2/1/2
	Ø.74ØØ	3Ø.ØØØØ	Ø.52ØØ	Ø.8829	Ø.ØØ282	9.455Ø	READ*
NACA—0012 (NASA 0.3-m TCT) (Averaged)	Ø.8ØØØ	6.ØØØØ	Ø.512Ø	Ø.8693	Ø.ØØ383	6.5ØØ2Ø	3/1/3
	Ø.74ØØ	9.ØØØØ	Ø.549Ø	Ø.9322	Ø.ØØ379	8.286Ø	2/1/2
	Ø.78ØØ	15.ØØØØ	Ø.47ØØ	Ø.798Ø	Ø.ØØ293	6.9595	READ*
	Ø.74ØØ	3Ø.ØØØØ	Ø.5183	Ø.88ØØ	Ø.ØØ281	9.4895	2/1/2

*READ - The $\langle C_p \rangle$ values are determined by manually reading the shifted C_p plots.

TABLE 4. (cont'd)

Airfoil	Mach	RexE06	Cp Jump	Cp Jump *	Cp Jump * / RE**.2	Slope	Terms
SC(3)-0712(b) (NASA 0.3-m TCT) (free transition)	Ø.78ØØ	1Ø.ØØØØ	Ø.541Ø	Ø.7982	Ø.Ø318	9.845Ø	2/1/2
	Ø.78ØØ	1Ø.ØØØØ	Ø.5439	Ø.8Ø25	Ø.Ø319	9.686Ø	2/2/2
	Ø.78ØØ	1Ø.ØØØØ	Ø.5512	Ø.8133	Ø.Ø324	9.255Ø	2/2/2
	Ø.79ØØ	1Ø.ØØØØ	Ø.5612	Ø.828Ø	Ø.Ø33Ø	9.7Ø1Ø	2/1/2
	Ø.79ØØ	1Ø.ØØØØ	Ø.5614	Ø.8283	Ø.Ø33Ø	9.715Ø	2/2/2
	Ø.8ØØØ	1Ø.ØØØØ	Ø.55Ø1	Ø.8116	Ø.Ø323	1Ø.Ø39Ø	2/1/2
	Ø.8ØØØ	1Ø.ØØØØ	Ø.5582	Ø.8236	Ø.Ø328	1Ø.141Ø	2/2/2
	Ø.78ØØ	15.ØØØØ	Ø.5741	Ø.847Ø	Ø.Ø311	1Ø.Ø44Ø	2/1/2
	Ø.78ØØ	15.ØØØØ	Ø.5768	Ø.851Ø	Ø.Ø312	1Ø.2Ø8Ø	2/2/2
	Ø.8ØØØ	15.ØØØØ	Ø.5622	Ø.8295	Ø.Ø3Ø5	13.792Ø	2/1/2
	Ø.8ØØØ	15.ØØØØ	Ø.5624	Ø.8298	Ø.Ø3Ø5	13.81ØØ	3/2/3
	Ø.78ØØ	3Ø.ØØØØ	Ø.6Ø8Ø	Ø.8971	Ø.Ø287	11.354Ø	2/1/2
	Ø.78ØØ	3Ø.ØØØØ	Ø.6Ø43	Ø.8916	Ø.Ø285	11.4Ø6Ø	2/1/2
	Ø.78ØØ	3Ø.ØØØØ	Ø.61Ø8	Ø.9Ø12	Ø.Ø288	11.474Ø	2/2/2
	Ø.79ØØ	3Ø.ØØØØ	Ø.5972	Ø.8811	Ø.Ø282	12.823Ø	2/1/2
	Ø.79ØØ	3Ø.ØØØØ	Ø.5966	Ø.88Ø2	Ø.Ø281	12.825Ø	2/2/2
	Ø.8ØØØ	3Ø.ØØØØ	Ø.5981	Ø.8825	Ø.Ø282	12.68ØØ	2/1/2
	Ø.8ØØØ	3Ø.ØØØØ	Ø.6Ø6Ø	Ø.8941	Ø.Ø286	12.528Ø	2/2/2
(fixed transition) (Averaged)	Ø.78ØØ	1Ø.ØØØØ	Ø.5488	Ø.8Ø97	Ø.Ø322	9.933Ø	2/1/2
	Ø.78ØØ	15.ØØØØ	Ø.5953	Ø.8783	Ø.Ø322	9.479Ø	2/1/2
	Ø.78ØØ	3Ø.ØØØØ	Ø.586Ø	Ø.8646	Ø.Ø276	12.526Ø	2/1/2
SC(3)-0712(b) (NASA 0.3-m TCT) (free transition) (Averaged)	Ø.78ØØ	1Ø.ØØØØ	Ø.555Ø	Ø.8115	Ø.Ø323	9.7689	2/1/2
	Ø.78ØØ	15.ØØØØ	Ø.57ØØ	Ø.841Ø	Ø.Ø3Ø5	11.9815	2/1/2
	Ø.78ØØ	3Ø.ØØØØ	Ø.6ØØØ	Ø.8852	Ø.Ø283	12.1557	2/1/2

TABLE 4. (cont'd)

Airfoil	Mach	RexE06	Cp Jump	Cp Jump *	Cp Jump * / RE**.2	Slope	Terms
CAST 10-2/DOA (NASA 0.3-m TCT)	Ø.78ØØ	4.ØØØØ	Ø.5316	Ø.8612	Ø.Ø412	9.1Ø9Ø	2/1/2
	Ø.78ØØ	4.ØØØØ	Ø.5271	Ø.8539	Ø.Ø4Ø8	9.135Ø	2/2/2
	Ø.79ØØ	4.ØØØØ	Ø.5122	Ø.8298	Ø.Ø397	9.212Ø	2/1/2
	Ø.79ØØ	4.ØØØØ	Ø.5267	Ø.8533	Ø.Ø4Ø8	8.753Ø	2/1/2
	Ø.8ØØØ	4.ØØØØ	Ø.545Ø	Ø.8829	Ø.Ø422	8.822Ø	2/1/2
	Ø.8ØØØ	4.ØØØØ	Ø.5448	Ø.8826	Ø.Ø422	8.819Ø	2/1/2
	Ø.8ØØØ	6.ØØØØ	Ø.5253	Ø.851Ø	Ø.Ø375	8.684Ø	2/1/2
	Ø.8ØØØ	6.ØØØØ	Ø.526Ø	Ø.8521	Ø.Ø376	8.662Ø	2/2/2
	Ø.78ØØ	1Ø.ØØØØ	Ø.524Ø	Ø.8489	Ø.Ø338	6.644Ø	2/1/2
	Ø.78ØØ	1Ø.ØØØØ	Ø.5299	Ø.8584	Ø.Ø342	6.849Ø	2/2/2
	Ø.79ØØ	1Ø.ØØØØ	Ø.491Ø	Ø.7954	Ø.Ø317	1Ø.928Ø	2/1/2
	Ø.79ØØ	1Ø.ØØØØ	Ø.49Ø8	Ø.7951	Ø.Ø317	1Ø.735Ø	2/2/2
	Ø.8ØØØ	1Ø.ØØØØ	Ø.53Ø7	Ø.8597	Ø.Ø342	7.854Ø	2/1/2
	Ø.8ØØØ	1Ø.ØØØØ	Ø.5274	Ø.8544	Ø.Ø34Ø	7.897Ø	2/2/2
	Ø.78ØØ	15.ØØØØ	Ø.5Ø81	Ø.8231	Ø.Ø3Ø2	7.895Ø	2/1/2
	Ø.78ØØ	15.ØØØØ	Ø.5Ø48	Ø.8178	Ø.Ø3ØØ	7.858Ø	2/2/2
	Ø.79ØØ	15.ØØØØ	Ø.56Ø5	Ø.9Ø8Ø	Ø.Ø333	8.493Ø	2/1/2
	Ø.79ØØ	15.ØØØØ	Ø.5549	Ø.8989	Ø.Ø33Ø	8.627Ø	2/2/2
	Ø.8ØØØ	15.ØØØØ	Ø.5694	Ø.9224	Ø.Ø339	9.546Ø	2/1/2
	Ø.8ØØØ	15.ØØØØ	Ø.5742	Ø.93Ø2	Ø.Ø341	9.7ØØØ	2/2/2
CAST 10-2/DOA (NASA 0.3-m TCT) (Averaged)	Ø.79ØØ	4.ØØØØ	Ø.531Ø	Ø.86Ø2	Ø.Ø411	8.9885	2/1/2
	Ø.8ØØØ	6.ØØØØ	Ø.526Ø	Ø.8521	Ø.Ø376	8.763Ø	2/1/2
	Ø.79ØØ	1Ø.ØØØØ	Ø.516Ø	Ø.8359	Ø.Ø333	6.9845	2/1/2
	Ø.79ØØ	15.ØØØØ	Ø.565Ø	Ø.9153	Ø.Ø336	8.6865	2/1/2

TABLE 4. (concluded)

Airfoil	Mach	RexE06	Cp Jump	Cp Jump *	Cp Jump * / RE**.2	Slope	Terms
DFVLR R-4 (NASA 0.3-m TCT)	Ø.78ØØ	4.ØØØØ	Ø.4645	Ø.6886	Ø.Ø329	26.1Ø3Ø	2/1/2
	Ø.78ØØ	4.ØØØØ	Ø.4642	Ø.6882	Ø.Ø329	26.413Ø	2/1/2
	Ø.78ØØ	15.ØØØØ	Ø.5393	Ø.7995	Ø.Ø293	1Ø.533Ø	2/1/2
	Ø.78ØØ	15.ØØØØ	Ø.5335	Ø.79Ø9	Ø.Ø29Ø	1Ø.8Ø7Ø	2/2/2
	Ø.78ØØ	4Ø.ØØØØ	Ø.59ØØ	Ø.8747	Ø.Ø264	15.Ø51Ø	READ*
DFVLR R-4 (NASA 0.3-m TCT) (Averaged)	Ø.78ØØ	4.ØØØØ	Ø.4645	Ø.6886	Ø.Ø329	26.2715	2/1/2
	Ø.78ØØ	15.ØØØØ	Ø.535Ø	Ø.7931	Ø.Ø291	1Ø.67ØØ	2/1/2
	Ø.78ØØ	4Ø.ØØØØ	Ø.59ØØ	Ø.8747	Ø.Ø264	15.Ø51Ø	READ*
CAST 7 (ARA Bedford)	Ø.76ØØ	6.ØØØØ	Ø.56ØØ	Ø.9785	Ø.Ø431	11.429Ø	READ*
MBB-A3 (ARA Bedford)	Ø.8ØØØ	6.ØØØØ	Ø.5135	Ø.9686	Ø.Ø427	5.533Ø	1/1/1
	Ø.8ØØØ	6.ØØØØ	Ø.5Ø57	Ø.9539	Ø.Ø421	5.533Ø	3/1/1
ONERA-D (TUNNEL 47/R1-CH)	Ø.81ØØ	4.5ØØØ	Ø.3249	Ø.6248	Ø.Ø292	9.911Ø	2/1/2
	Ø.84ØØ	4.5ØØØ	Ø.3446	Ø.6627	Ø.Ø31Ø	7.953Ø	2/1/2
12% BI-CONVEX	Ø.823Ø	Ø.76ØØ	Ø.54ØØ	Ø.8893	Ø.Ø593	Ø.ØØØØ	READ*
18% BI-CONVEX	Ø.78ØØ	1Ø.3ØØØ	Ø.54ØØ	Ø.6867	Ø.Ø272	Ø.ØØØØ	READ*
	Ø.78ØØ	17.ØØØØ	Ø.54ØØ	Ø.6867	Ø.Ø246	Ø.ØØØØ	READ*

*READ - The $\langle C_p \rangle$ values are determined by manually reading the shifted C_p plots.

TABLE 5. GEOMETRIC CHARACTERISTICS FOR THE TWO-DIMENSIONAL AIRFOILS

Airfoil	max(t/c)	Rle/c (rle*)	Upper crest x/c	Upper crest (1/R)	Low surf DelTEL	Camber Surf DelTEC
NACA--0012	0.1200	0.0158	0.3000	0.4520	-0.1390	0.0000
SC(3)-0712(b)	0.1210	0.0093	0.4000	0.2930	0.2480	0.2650
CAST 10-2/DOA 2	0.1238	0.0122	0.3950	0.3800	-0.0300	0.1050
DFVLR R4	0.1350	0.0210	0.3890	0.3030	0.2050	0.2510
CAST 7	0.1170	0.0115	0.4120	0.2840	0.0870	0.1490
MBB-A3	0.0890	0.0075	0.3910	0.3300	-0.0124	0.0560
ONERA-D	0.3700	0.0145	0.3650	0.3750	-0.1530	0.0000
12% BI-CONVEX	0.1200	0.0000	0.5000	0.4732	0.0000	0.0000
18% BI-CONVEX	0.1800	0.0000	0.5000	0.6974	0.0000	0.0000

TABLE 6. TABULATED C_p JUMP RESULTS FOR THREE-DIMENSIONAL CONFIGURATION DATA

Airfoil	Mach	RexE06	Cp Jump	Cp Jump *	Cp Jump * / RE**.2	Slope	Terms
ONERA M-6 WING	Ø.8800	12.0000	Ø.4275	Ø.8793	Ø.Ø338	7.9220	2/1/2
(ONERA "D" AIRFIOL)	Ø.8800	12.0000	Ø.4291	Ø.8826	Ø.Ø339	8.0590	3/2/3
ONERA S2MA TWT							
	Ø.9300	12.0000	Ø.4183	Ø.8604	Ø.Ø330	7.2220	1/1/1
	Ø.9300	12.0000	Ø.3872	Ø.7964	Ø.Ø306	7.1590	2/2/2
	Ø.9300	12.0000	Ø.3866	Ø.7952	Ø.Ø305	7.1560	3/2/3
	Ø.9300	12.0000	Ø.4072	Ø.8375	Ø.Ø321	6.7930	1/1/1
	Ø.9300	12.0000	Ø.3985	Ø.8197	Ø.Ø315	6.6530	3/2/3
F-16 1/9th	Ø.9000	2.5000	Ø.3569	Ø.7842	Ø.Ø412	5.8810	1/1/1
(AEDC PWT-16T)	Ø.9000	2.5000	Ø.4200	Ø.9229	Ø.Ø485	5.8810	Read*
	Ø.9100	2.5000	Ø.4248	Ø.9335	Ø.Ø490	5.0800	1/1/1
	Ø.9100	2.5000	Ø.4300	Ø.9449	Ø.Ø496	5.0800	Read *
	Ø.9200	2.5000	Ø.4538	Ø.9972	Ø.Ø524	5.3350	1/1/1
	Ø.9200	2.5000	Ø.4400	Ø.9669	Ø.Ø508	5.0800	Read*
	Ø.9300	2.5000	Ø.3758	Ø.8258	Ø.Ø434	6.4520	2/1/2
	Ø.9300	2.5000	Ø.3900	Ø.8570	Ø.Ø450	6.4520	Read*
MBB Wing/Body	Ø.9000	1.3400	Ø.4624	Ø.9967	Ø.Ø593	4.3280	1/1/1
ARA Polytechnic	Ø.9000	1.3400	Ø.4800	1.0346	Ø.Ø616	4.3280	Read
C-141	Ø.8400	45.0000	Ø.5600	Ø.9691	Ø.Ø286	Ø.0000	Read*
(W-T and Flgt)	Ø.8400	59.0000	Ø.5900	1.0210	Ø.Ø285	Ø.0000	Read*
	Ø.8500	20.0000	Ø.5660	Ø.9794	0.0339	Ø.0000	Read*
	Ø.8500	58.0000	Ø.6300	1.0902	0.0305	Ø.0000	Read*
C-5A	Ø.7750	8.0000	Ø.5900	Ø.9632	Ø.Ø401	Ø.0000	READ*
(2 w-t & 1 flght)	Ø.7750	8.0000	Ø.5700	Ø.9306	Ø.Ø387	Ø.0000	READ*
	Ø.8500	80.0000	Ø.6170	1.0073	0.0265	Ø.0000	READ*

*READ - The <C_p> values are determined by manually reading the shifted C_p plots.

TABLE 7. GEOMETRIC CHARACTERISTICS FOR THE THREE-DIMENSIONAL CONFIGURATIONS

Configuration	max(t/c)	Rle/c (rle*)	Upper crest x/c	Upper crest (1/R)	Low surf DelTEL	Camber Surf DelTEC	Sweep
ONERA M-6 WING (Onera "d" airfoil)	Ø.Ø978	Ø.Ø145	Ø.376Ø	Ø.339Ø	-Ø.124Ø	Ø.ØØØØ	3Ø.ØØØØ
F-16 1/9th scale	Ø.Ø5ØØ	Ø.ØØ11	Ø.4ØØØ	Ø.262Ø	-Ø.Ø342	Ø.Ø45Ø	4Ø.ØØØØ
MBB WING/BODY	Ø.Ø834	Ø.ØØ75	Ø.392Ø	Ø.27ØØ	-Ø.124Ø	Ø.Ø46Ø	35.ØØØØ
F-111 TACT	Ø.ØØØØ	Ø.ØØØØ	Ø.3ØØØ	Ø.137Ø	Ø.1664	Ø.2641	26.ØØØØ
C-141	Ø.1ØØØ	Ø.Ø11Ø	Ø.4ØØØ	Ø.39ØØ	-Ø.Ø996	Ø.Ø493	27.ØØØØ
C-5A	Ø.1ØØØ	Ø.Ø133	Ø.425Ø	Ø.391Ø	-Ø.1Ø81	Ø.Ø884	27.39ØØ

TABLE 8. TABULATED ONSET RESULTS FOR TWO-DIMENSIONAL AIRFOIL DATA

Airfoil	Mach	RexE06	AlphaTW	AlphaTED	Sep Ind*	A	AlphaTED A=Ø.19Ø
NACA—0012 (NASA 0.3-m TCT)	Ø.76ØØ	6.ØØØØ	Ø.ØØØØ	5.Ø5ØØ	Ø.Ø	Ø.19ØØ	5.Ø5ØØ
	Ø.8ØØØ	6.ØØØØ	Ø.ØØØØ	4.ØØØØ	1.Ø	Ø.19Ø5	4.1ØØØ
	Ø.82ØØ	6.ØØØØ	Ø.ØØØØ	3.Ø1ØØ	-1.Ø	Ø.192Ø	3.3ØØØ
	Ø.74ØØ	9.ØØØØ	Ø.ØØØØ	6.Ø5ØØ	1.Ø	Ø.1862	5.3ØØØ
	Ø.76ØØ	15.ØØØØ	Ø.ØØØØ	5.Ø2ØØ	-1.Ø	Ø.19Ø2	5.Ø3ØØ
	Ø.78ØØ	15.ØØØØ	Ø.ØØØØ	5.Ø3ØØ	1.Ø	Ø.1879	4.7ØØØ
	Ø.8ØØØ	15.ØØØØ	Ø.ØØØØ	4.Ø4ØØ	-1.Ø	Ø.19Ø2	4.1ØØØ
	Ø.74ØØ	3Ø.ØØØØ	Ø.ØØØØ	5.Ø6ØØ	-1.Ø	Ø.1914	5.3ØØØ
SC(3)-0712(b) (NASA 0.3-m TCT) (free transition)	Ø.78ØØ	1Ø.ØØØØ	Ø.ØØØØ	1.52ØØ	Ø.Ø	Ø.19Ø1	1.55ØØ
	Ø.79ØØ	1Ø.ØØØØ	Ø.ØØØØ	1.Ø1ØØ	Ø.Ø	Ø.1914	1.2ØØØ
	Ø.8ØØØ	1Ø.ØØØØ	Ø.ØØØØ	Ø.51ØØ	1.Ø	Ø.1925	Ø.9ØØØ
	Ø.78ØØ	15.ØØØØ	Ø.ØØØØ	1.53ØØ	Ø.Ø	Ø.19Ø1	1.55ØØ
	Ø.8ØØØ	15.ØØØØ	Ø.ØØØØ	1.Ø3ØØ	1.Ø	Ø.1896	Ø.9ØØØ
	Ø.78ØØ	3Ø.ØØØØ	Ø.ØØØØ	1.51ØØ	Ø.Ø	Ø.19Ø2	1.55ØØ
	Ø.79ØØ	3Ø.ØØØØ	Ø.ØØØØ	1.Ø1ØØ	Ø.Ø	Ø.1914	1.2ØØØ
	Ø.8ØØØ	3Ø.ØØØØ	Ø.ØØØØ	1.Ø2ØØ	1.Ø	Ø.1896	Ø.9ØØØ
(fixed transition)	Ø.78ØØ	1Ø.ØØØØ	Ø.ØØØØ	1.5ØØØ	-1.Ø	Ø.19Ø2	1.55ØØ
	Ø.78ØØ	15.ØØØØ	Ø.ØØØØ	1.53ØØ	-1.Ø	Ø.19Ø1	1.55ØØ
	Ø.78ØØ	3Ø.ØØØØ	Ø.ØØØØ	1.51ØØ	Ø.Ø	Ø.19Ø2	1.55ØØ

*Key to seperation indicator: -1 = Before shock induced trailing edge seperation
Ø = At shock induced trailing edge seperation
1 = After shock induced trailing edge seperation

TABLE 8. (concluded)

Airfoil	Mach	RexE06	AlphaTW	AlphaTED	Sep Ind*	A	AlphaTED A=Ø.19Ø
CAST 10-2/DOA (NASA 0.3-m TCT)	Ø.78ØØ	4.ØØØØ	Ø.ØØØØ	1.Ø3ØØ	Ø.Ø	Ø.1922	1.4ØØØ
	Ø.79ØØ	4.ØØØØ	Ø.ØØØØ	Ø.Ø5ØØ	1.Ø	Ø.1944	1.1ØØØ
	Ø.8ØØØ	4.ØØØØ	Ø.ØØØØ	Ø.Ø1ØØ	-1.Ø	Ø.1961	Ø.9ØØØ
	Ø.8ØØØ	6.ØØØØ	Ø.ØØØØ	1.Ø3ØØ	1.Ø	Ø.189Ø	Ø.9ØØØ
	Ø.78ØØ	1Ø.ØØØØ	Ø.ØØØØ	1.5ØØØ	1.Ø	Ø.1891	1.4ØØØ
	Ø.79ØØ	1Ø.ØØØØ	Ø.ØØØØ	1.Ø4ØØ	-1.Ø	Ø.19Ø7	1.1ØØØ
	Ø.8ØØØ	1Ø.ØØØØ	Ø.ØØØØ	1.Ø3ØØ	1.Ø	Ø.189Ø	Ø.9ØØØ
	Ø.78ØØ	15.ØØØØ	Ø.ØØØØ	1.52ØØ	Ø.Ø	Ø.189Ø	1.4ØØØ
	Ø.79ØØ	15.ØØØØ	Ø.ØØØØ	1.Ø5ØØ	Ø.Ø	Ø.19Ø6	1.1ØØØ
	Ø.8ØØØ	15.ØØØØ	Ø.ØØØØ	1.Ø3ØØ	1.Ø	Ø.189Ø	Ø.9ØØØ
DFVLR R-4 (NASA 0.3-m TCT)	Ø.78ØØ	4.ØØØØ	Ø.ØØØØ	Ø.ØØØØ	1.Ø	Ø.1988	1.5ØØØ
	Ø.78ØØ	15.ØØØØ	Ø.ØØØØ	Ø.5ØØØ	Ø.Ø	Ø.1958	1.5ØØØ
	Ø.78ØØ	4Ø.ØØØØ	Ø.ØØØØ	Ø.51ØØ	Ø.Ø	Ø.1958	1.5ØØØ
CAST 7 (ARA Bedford)	Ø.76ØØ	6.ØØØØ	Ø.ØØØØ	1.5ØØØ	-1.Ø	Ø.2ØØ7	3.ØØØØ
MBB-A3 (ARA Bedford)	Ø.76ØØ	6.ØØØØ	Ø.ØØØØ	3.73ØØ	-1.Ø	Ø.198Ø	4.9ØØØ
	Ø.76ØØ	6.ØØØØ	Ø.ØØØØ	4.74ØØ	1.Ø	Ø.19Ø9	4.9ØØØ
	Ø.8ØØØ	6.ØØØØ	Ø.ØØØØ	3.ØØØØ	Ø.Ø	Ø.1979	4.ØØØØ
	Ø.8ØØØ	6.ØØØØ	Ø.ØØØØ	4.47ØØ	1.Ø	Ø.1873	4.ØØØØ
	Ø.85ØØ	6.ØØØØ	Ø.ØØØØ	2.ØØØØ	1.Ø	Ø.1922	2.2ØØØ
ONERA-D (TUNNEL 47/R1-CH)	Ø.81ØØ	4.5ØØØ	Ø.ØØØØ	6.ØØØØ	-1.Ø	Ø.1651	Ø.ØØØØ
	Ø.85ØØ	4.5ØØØ	Ø.ØØØØ	4.ØØØØ	-1.Ø	Ø.1672	Ø.ØØØØ

*Key to seperation indicator: -1 = Before shock induced trailing edge seperation
Ø = At shock induced trailing edge seperation
1 = After shock induced trailing edge seperation

TABLE 9. TABULATED ONSET RESULTS FOR THE THREE-DIMENSIONAL CONFIGURATIONS

Airfoil	Mach	RexE06	AlphaTW	AlphaTED	Sep Ind*	A	AlphaTED A=Ø.19Ø
ONERA M-6 WING (ONERA "D" AIRFIOL)	Ø.8800	12.0000	Ø.0000	6.0000	Ø.Ø	Ø.1759	4.0000
ONERA S2MA TWT (free transition)	Ø.9200	12.0000	Ø.0000	5.0000	-1.Ø	Ø.1783	3.5000
	Ø.9200	12.0000	Ø.0000	6.0000	1.Ø	Ø.1717	3.5000
F-16 1/9th (AEDC PWT-16T) (fixed transition)	Ø.9000	2.5000	-2.0000	7.5600	1.Ø	Ø.1848	6.9000
	Ø.9100	2.5000	-2.0000	7.5700	Ø.Ø	Ø.1849	6.9000
	Ø.9200	2.5000	-2.0000	7.5700	1.Ø	Ø.1850	6.9000
	Ø.9300	2.5000	-2.0000	7.5800	1.Ø	Ø.1849	6.9000
MBB Wing/Body	Ø.8800	1.3400	Ø.0000	4.0000	1.Ø	Ø.1692	1.5000
ARA Polytechnic (free transition)	Ø.9200	1.3400	Ø.0000	2.0000	Ø.Ø	Ø.1839	1.4000
F-111 TACT	Ø.8540	2.3000	-5.0000	10.2000	1.Ø	Ø.1894	10.1000
(fixed transition)	Ø.8540	2.3000	-5.0000	8.2000	Ø.Ø	Ø.2013	10.1000
	Ø.9000	2.3000	-5.0000	8.2000	1.Ø	Ø.1946	9.0000
	Ø.8500	7.0000	-5.0000	8.4000	-1.Ø	Ø.2005	10.1000
	Ø.8500	7.0000	-5.0000	10.3000	1.Ø	Ø.1895	10.3000
	Ø.9000	7.0000	-5.0000	10.2000	1.Ø	Ø.1831	9.0000
C-141 (W-T free transition)	Ø.8500	20.0000	1.1100	Ø.0000	Ø.Ø	Ø.1973	1.0000
(flt test)	Ø.8400	45.0000	1.1100	Ø.3100	Ø.Ø	Ø.1956	1.1000
	Ø.8400	59.0000	1.1100	1.0000	Ø.Ø	Ø.1905	1.1000
	Ø.8500	58.0000	1.1100	1.0000	Ø.Ø	Ø.1898	1.0000
C-5A	Ø.7750	8.0000	-2.34000	4.0000	1.Ø	Ø.1767	2.1000
(fixed tran)	Ø.7750	8.0000	-2.34000	2.0000	-1.Ø	Ø.1906	2.1000

*Key to seperation indicator: -1 = Before shock induced trailing edge seperation
Ø = At shock induced trailing edge seperation
1 = After shock induced trailing edge seperation

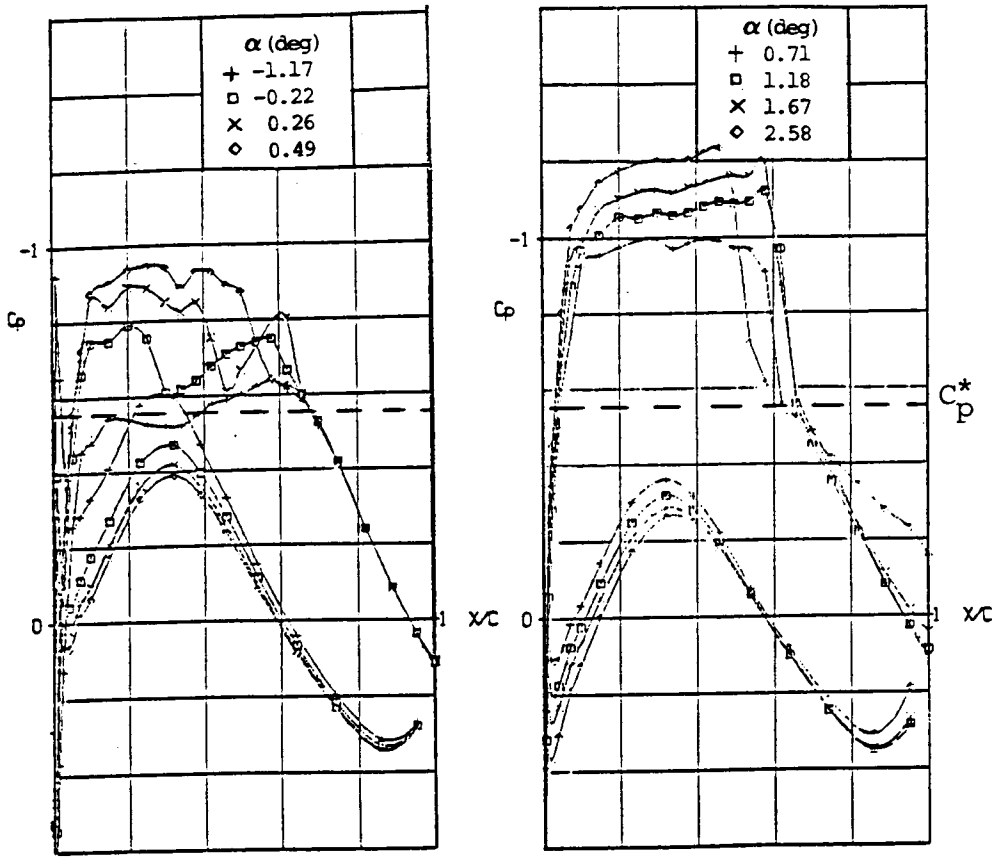

Figure 1 Two-Dimensional Pressure Data on a Supercritical CAST 7 Airfoil, M=0.76, R_e=6x10^6. (Reference 3)

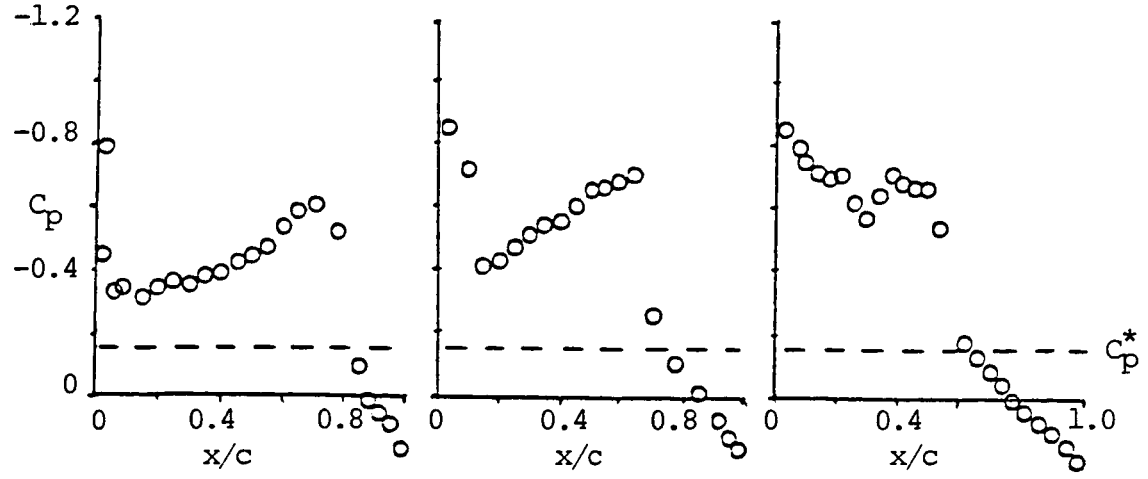

a) η=0.2 b) η=0.65 c) η=0.9

Figure 2 Upper Surface Pressure Distributions on the ONERA M-6 Wing, M=0.92, α=2 deg. (Reference 3)

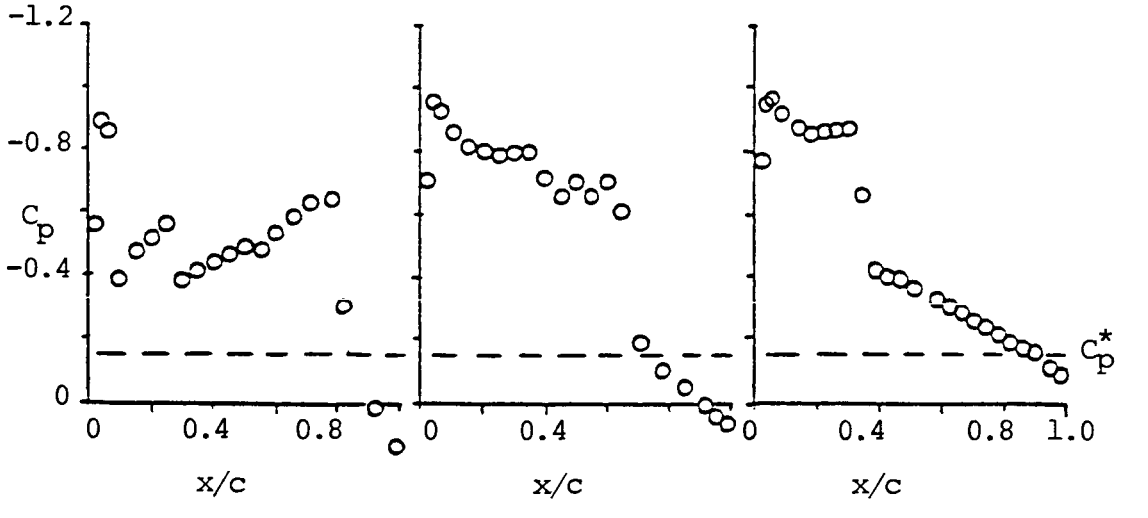

a) η=0.2 b) η=0.65 c) η=0.9

Figure 3 Upper Surface Pressure Distributions on the ONERA M-6 Wing, M=0.92, α=4 deg. (Reference 3)

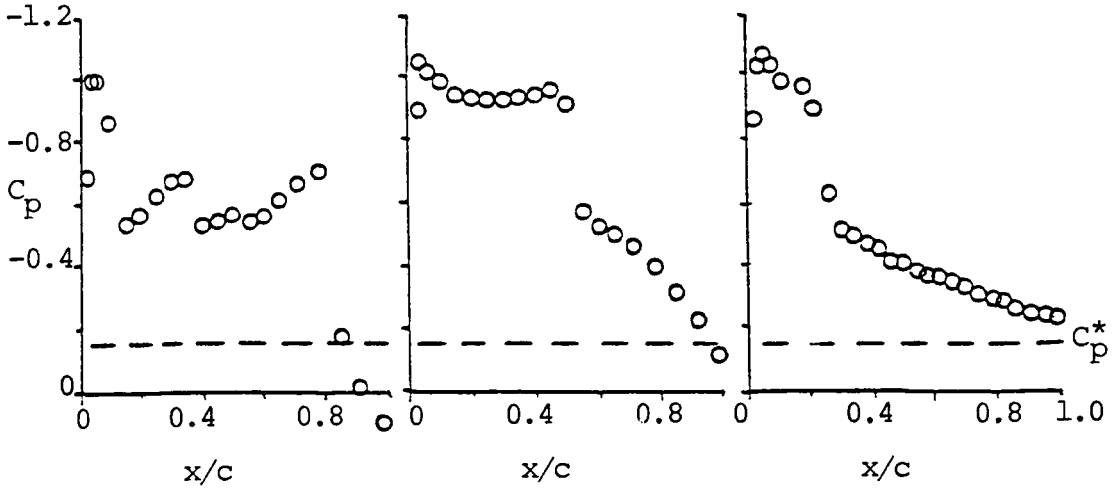

a) η=0.2 b) η=0.65 c) η=0.9

Figure 4 Upper Surface Pressure Distributions on the ONERA M-6 Wing, M=0.92, α=6 deg. (Reference 3)

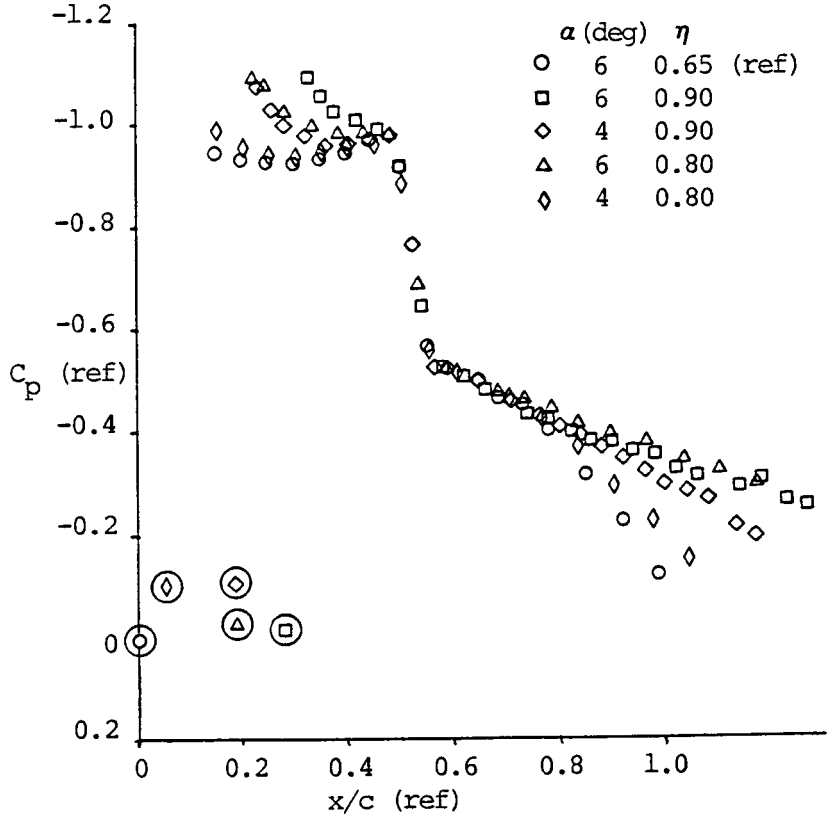

Figure 5 Shock Jump Similarity for the ONERA M-6 Wing Upper Surface Pressures at M=0.92, α=4 deg. and 6 deg., R_e=11.7x10^6. (Reference 3)

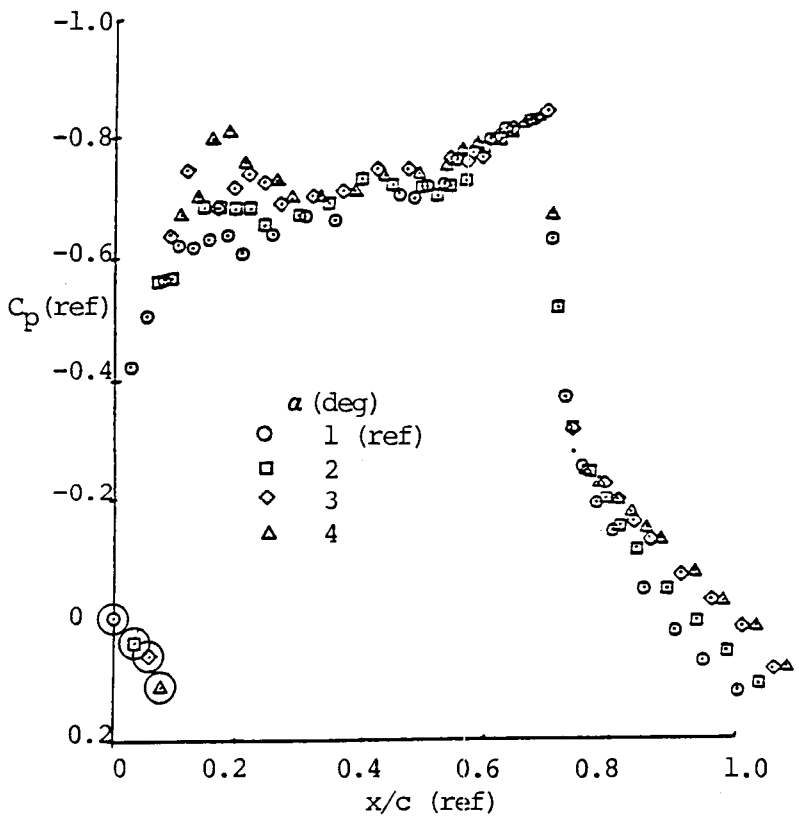

Figure 6 Shock Jump Similarity on the C-141 Upper Surface Pressures, M=0.85, R_e=20x10^6, η=0.193. (Reference 5)

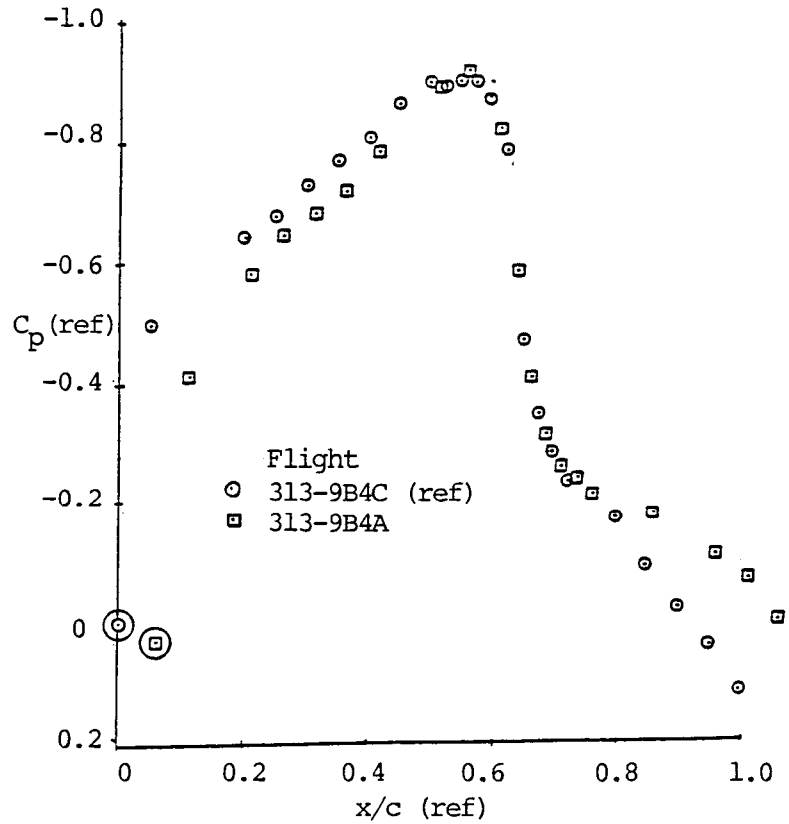

Figure 7 Shock Jump Similarity on the C-5A Upper Surface Wing Pressures, M=0.85, R_e=80x10^6, η=0.70. (Reference 5)

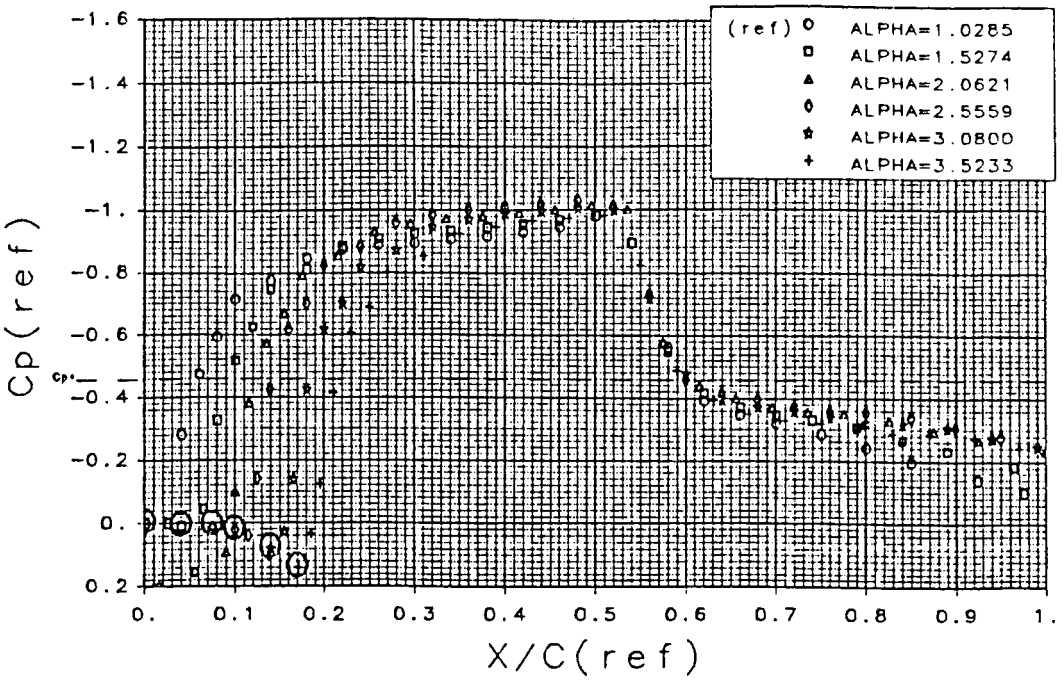

Figure 8 Shifted C_p Plot Format, CAST 10-2/DOA 2 Airfoil, M=0.78, R_e=4.01x10^6 (Reference 7)

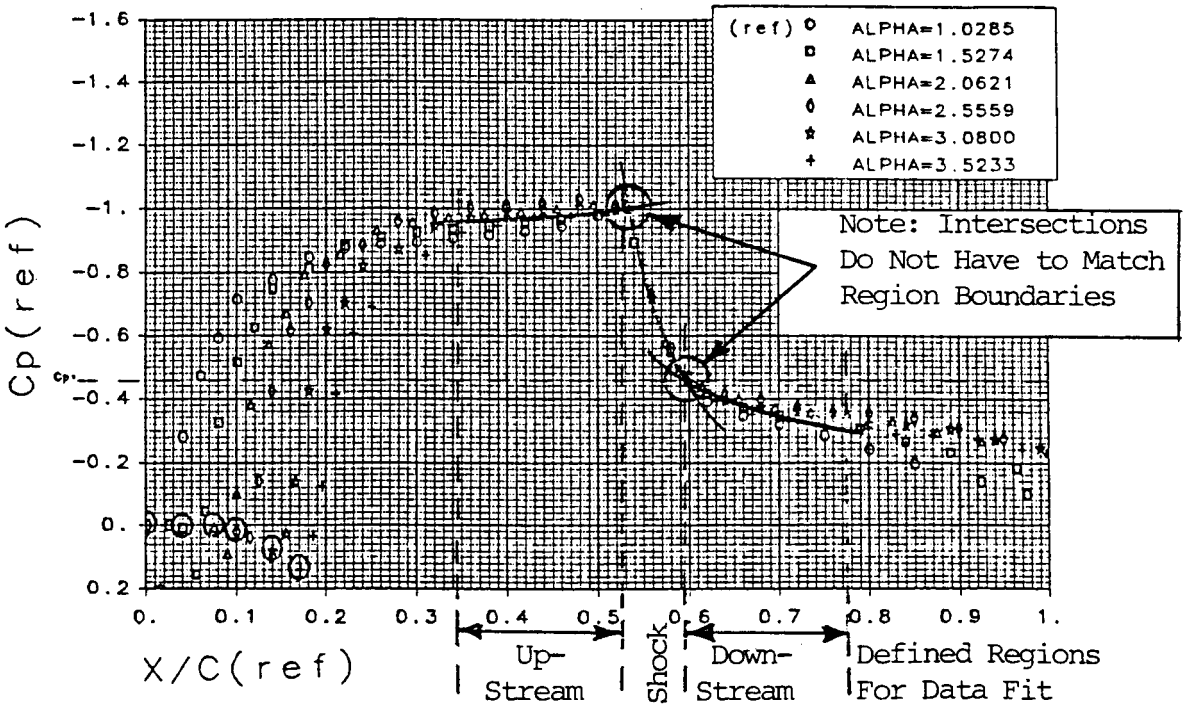

Figure 9 Scheme for Determining Shock Jump C_p Values from Shifted C_p Plots, CAST 10-2/DOA 2 Airfoil, M=0.78, R_e=4.01x10^6 (Reference 7)

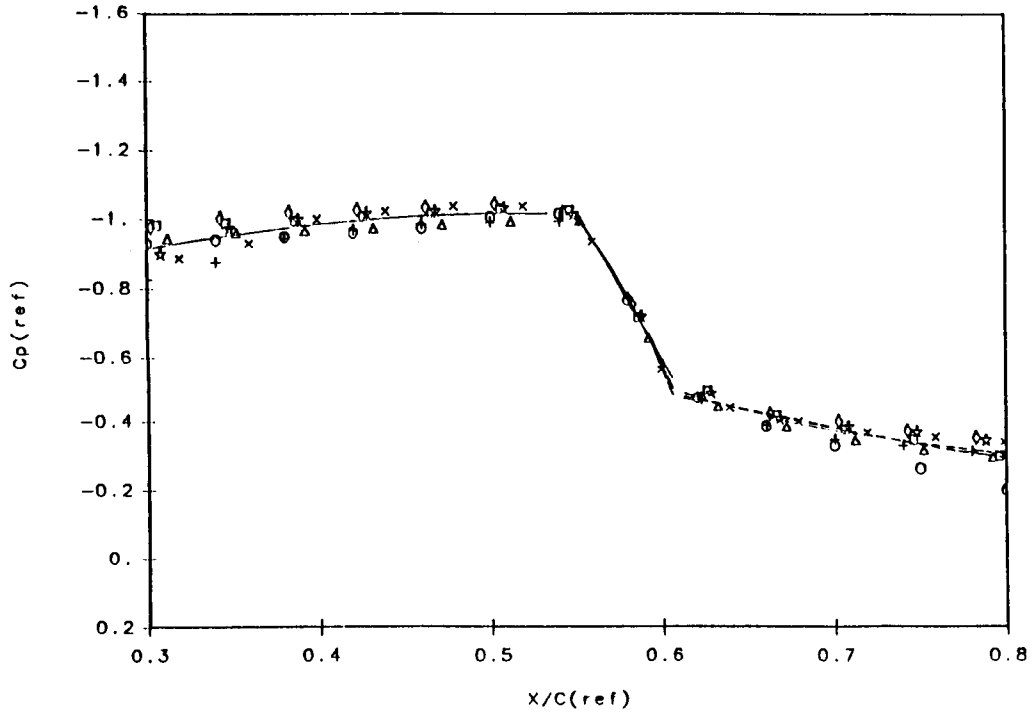

Delta Cp	Slope	Degree of fit 1	2	3
Ø.5372	8.629	2	1	2
Ø.53Ø9	8.987	2	2	2
Ø.531Ø	8.985	2	3	2
Ø.5448	8.629	3	1	3
Ø.54Ø5	9.Ø33	3	2	3
Ø.54Ø5	9.Ø3Ø	3	3	3
Ø.5216	8.629	4	1	4
Ø.5119	8.922	4	2	4
Ø.5Ø79	8.858	4	4	4

Figure 10 Sample Plot for Determining Shock Jump C_p Values from Shifted C_p Plots, CAST 10-2/DOA 2 Airfoil, M=0.78, R_e=4.01x10^6 (Reference 7)

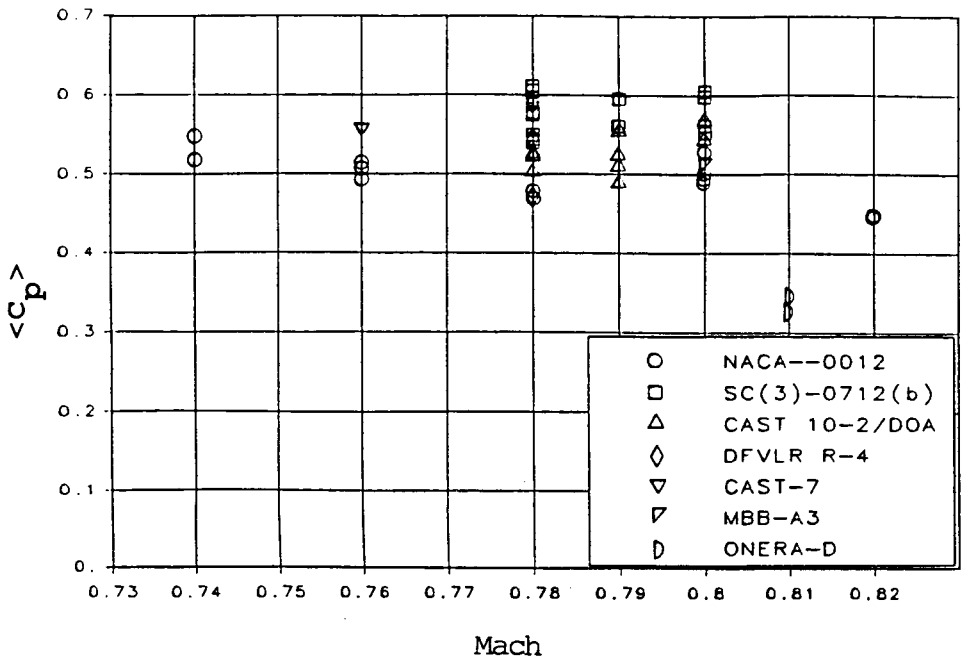

Figure 11 Influence of Mach Number on $\langle C_p \rangle$ for Raw Data in Two-Dimensional Flow

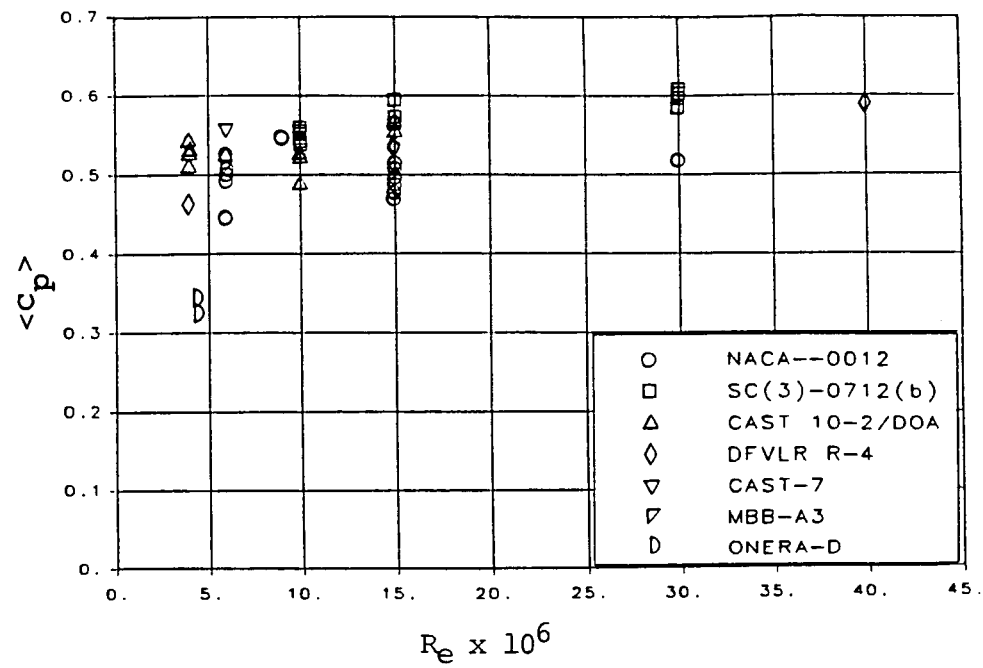

Figure 12 Influence of Reynolds Number on $\langle C_p \rangle$ for Raw Data in Two-Dimensional Flow

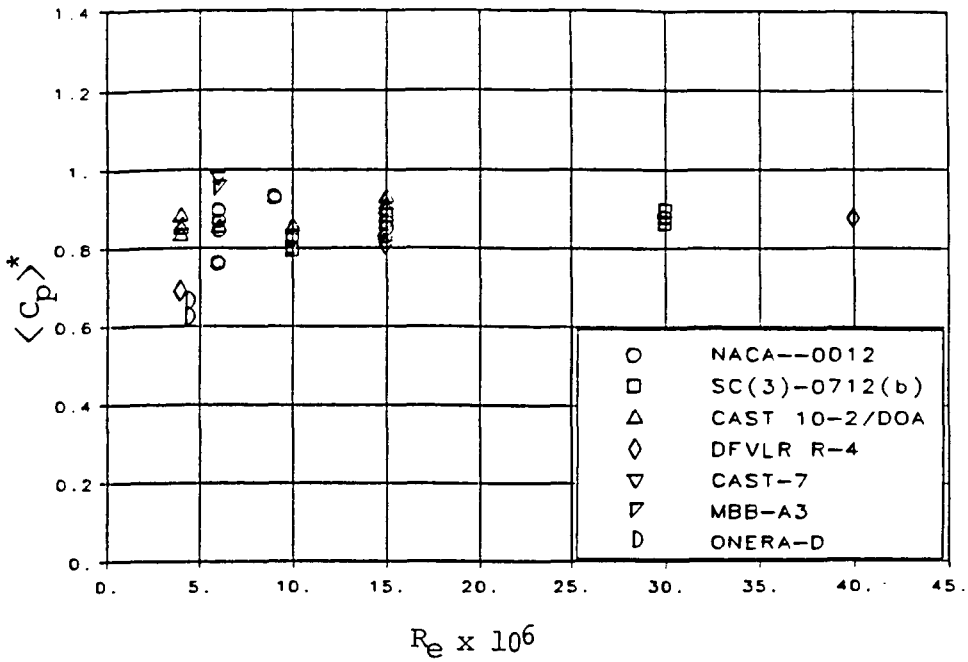

Figure 13 Influence of Reynolds Number on $\langle C_p \rangle^*$ for Raw Data in Two-Dimensional Flow

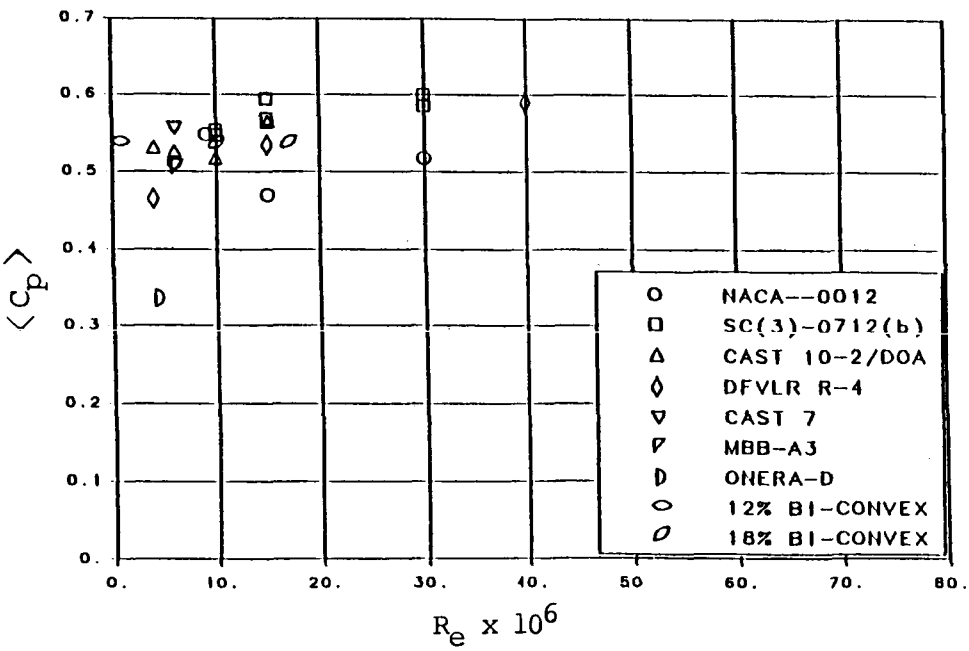

Figure 14 Influence of Reynolds Number on $\langle C_p \rangle$ for Averaged Data in Two-Dimensional Flow

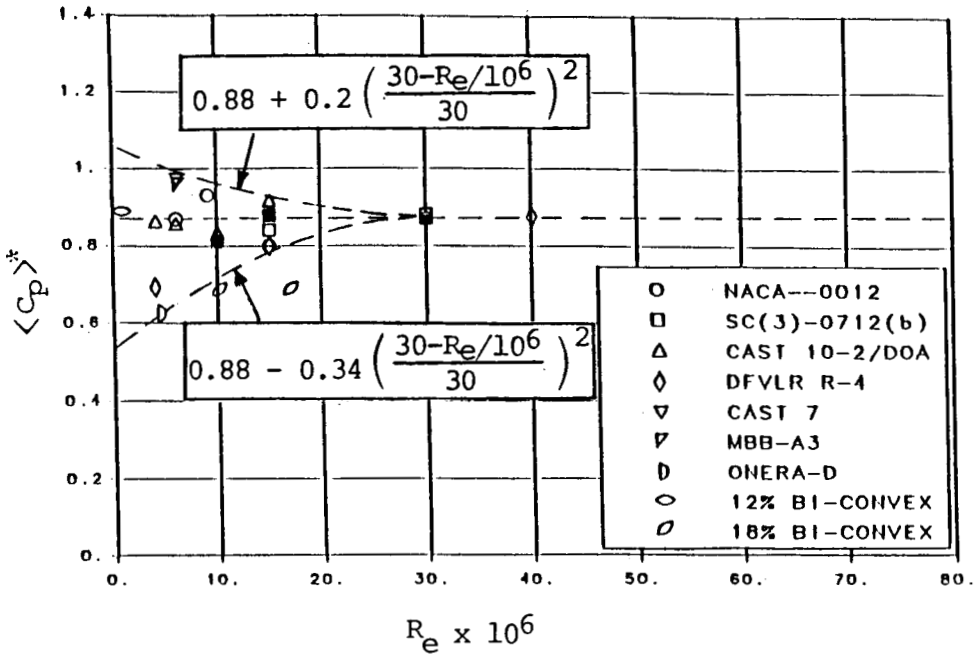

Figure 15 Influence of Reynolds Number on $\langle C_p \rangle^*$ for Averaged Data in Two-Dimensional Flow

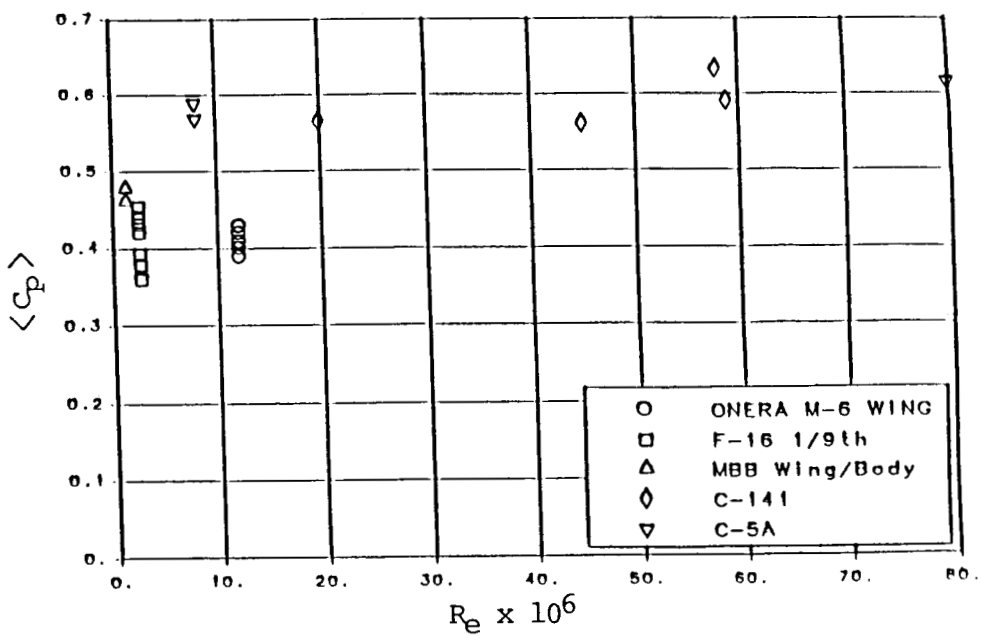

Figure 16 Influence of Reynolds Number on $\langle C_p \rangle$ for Raw Data in Three-Dimensional Flow

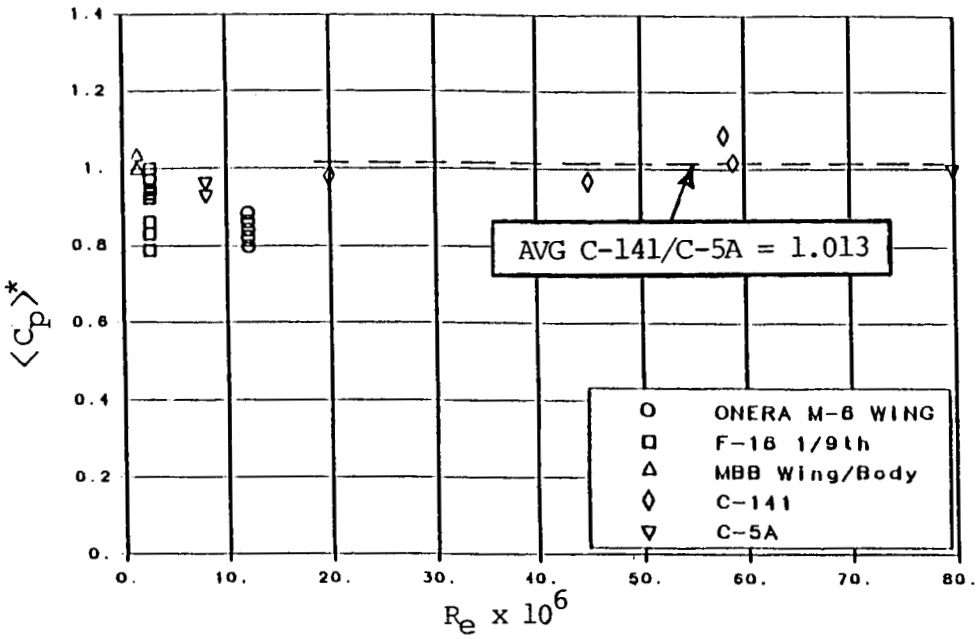

Figure 17 Influence of Reynolds Number on $\langle C_p \rangle^*$ for Raw Data in Three-Dimensional Flow

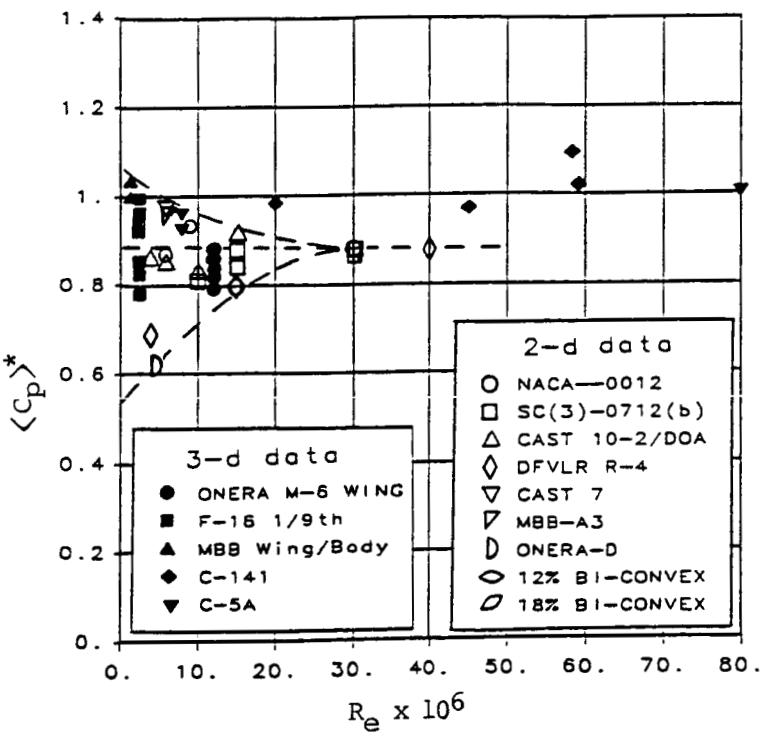

Figure 18 Influence of Reynolds Number on $\langle C_p \rangle^*$ for all Two- and Three-Dimensional Flow Data

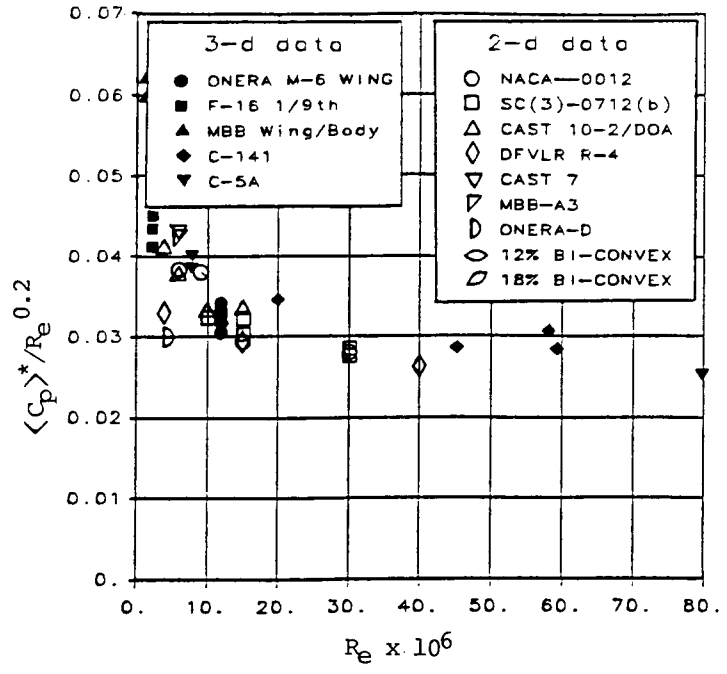

Figure 19 Influence of Reynolds Number on $\langle C_p \rangle^* / R_e^{0.2}$ for all Two- and Three-Dimensional Flow Data

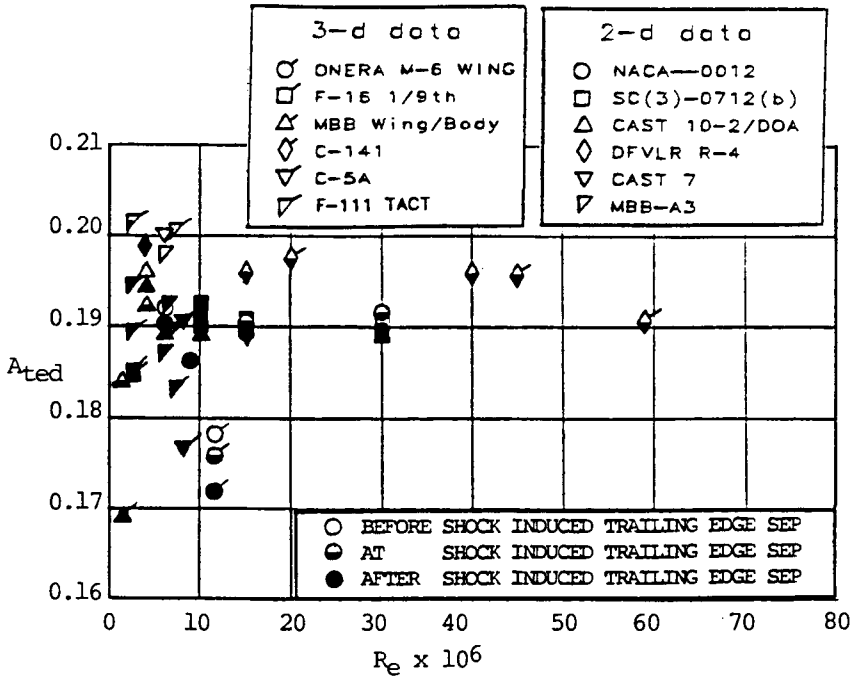

Figure 20 Influence of Reynolds Number on the SITES Onset Indicator, A_{ted}, for Two- and Three-Dimensional Flows

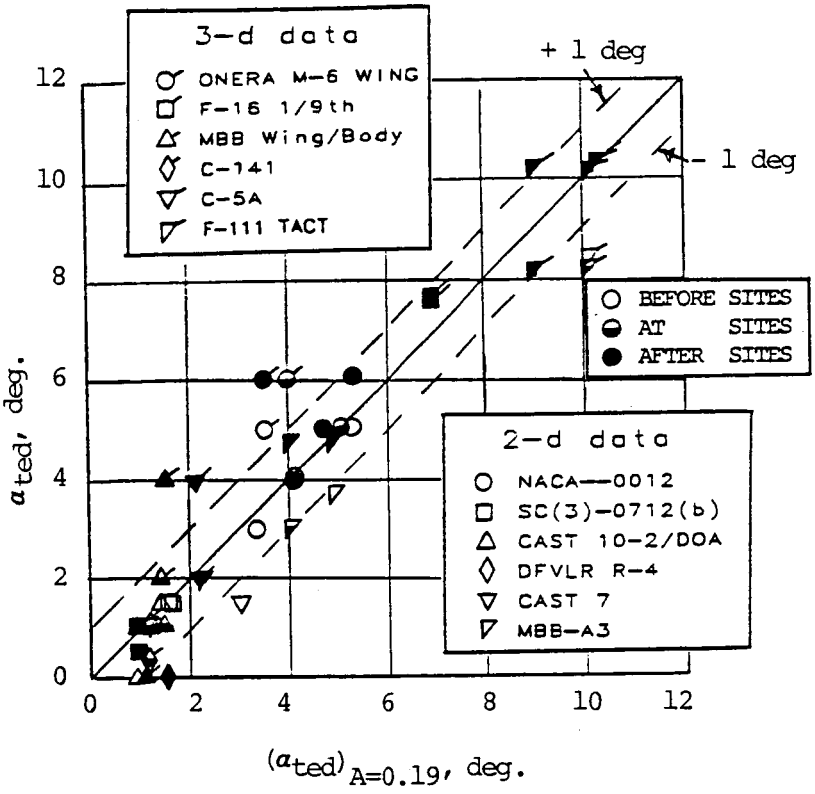

Figure 21 Evaluation of A_{ted}=0.19 for Predicting SITES Onset

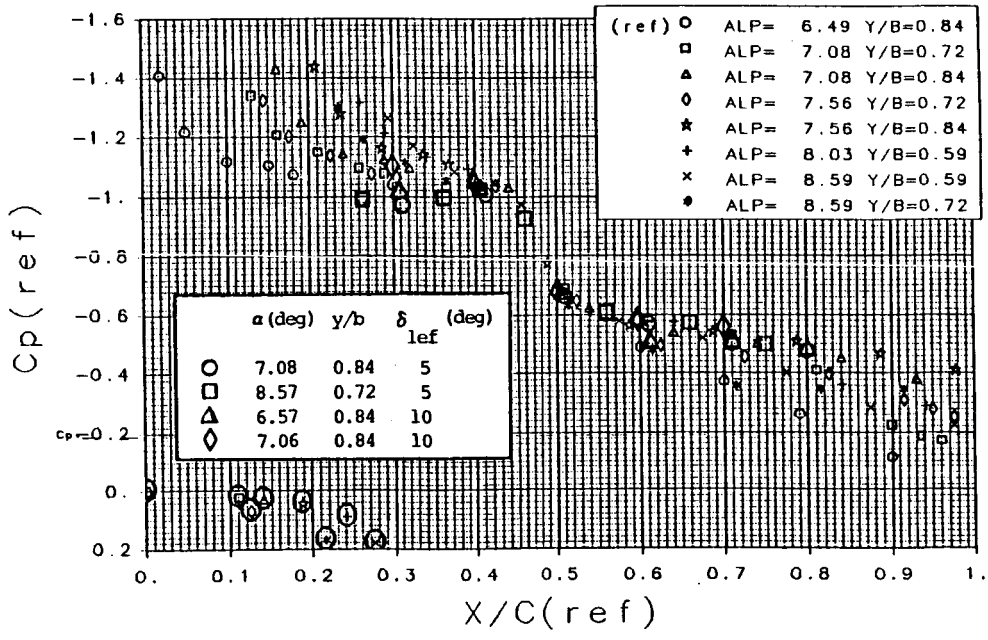

Figure 22 Influence of Leading Edge Flap Deflection on Shifted C_p Data for the F-16 Pressure Model, M=0.90, R_e=2.5x10^6

APPENDIX

Shifted C_p Plots

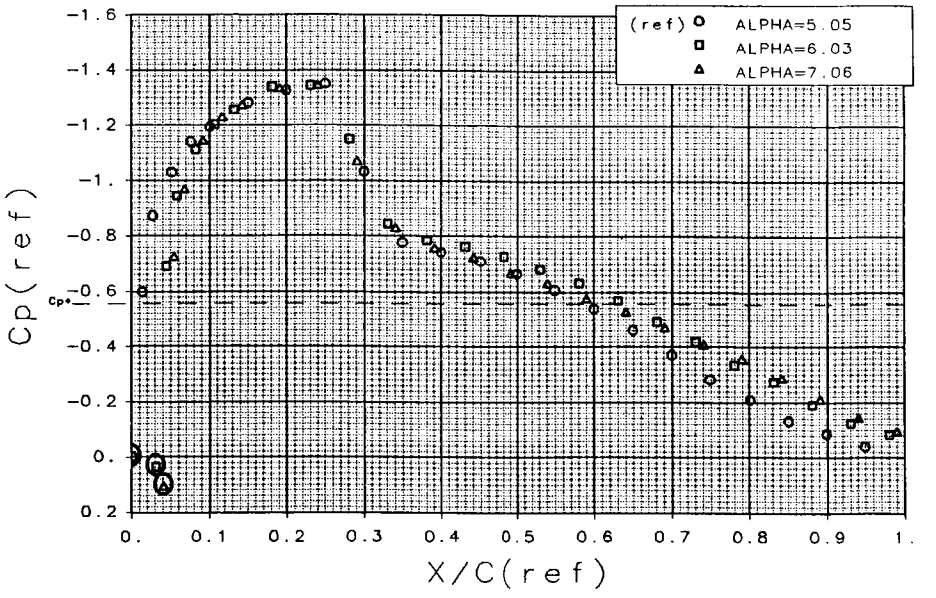

Figure A-1 NACA 0012 Airfoil, M=0.76, R_e=6x10^6

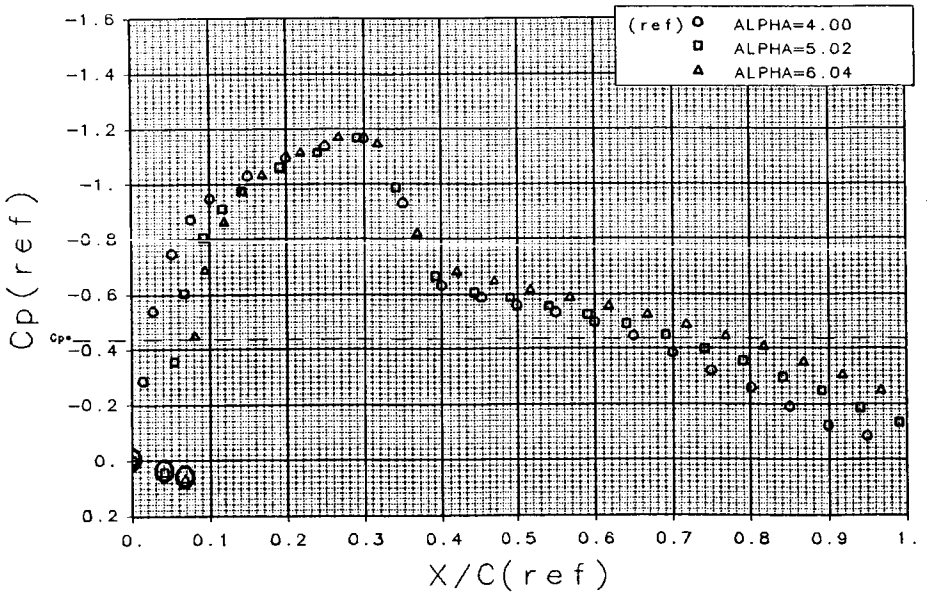

Figure A-2 NACA 0012 Airfoil, M=0.80, R_e=6x10^6

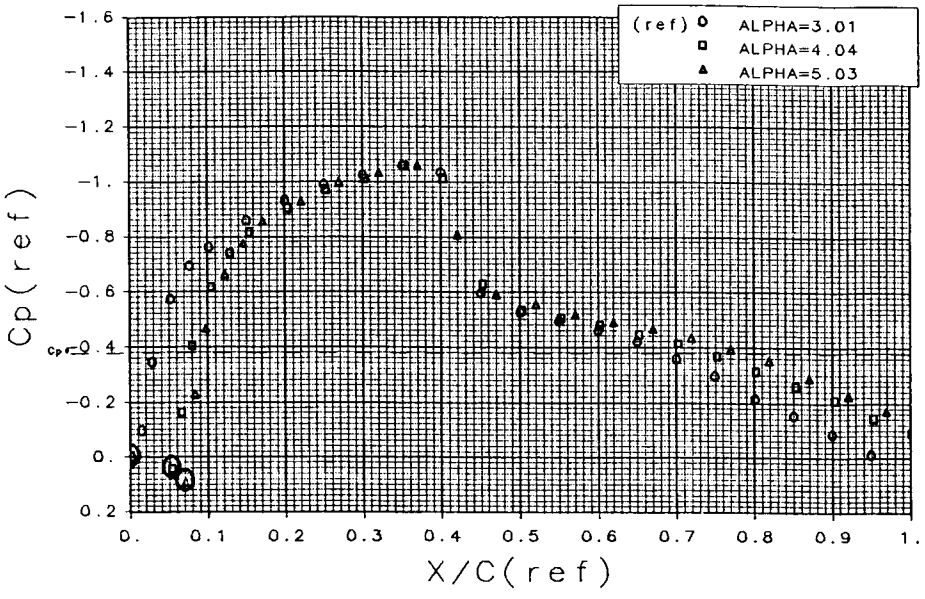

Figure A-3 NACA 0012 Airfoil, M=0.82, R_e=6x10^6

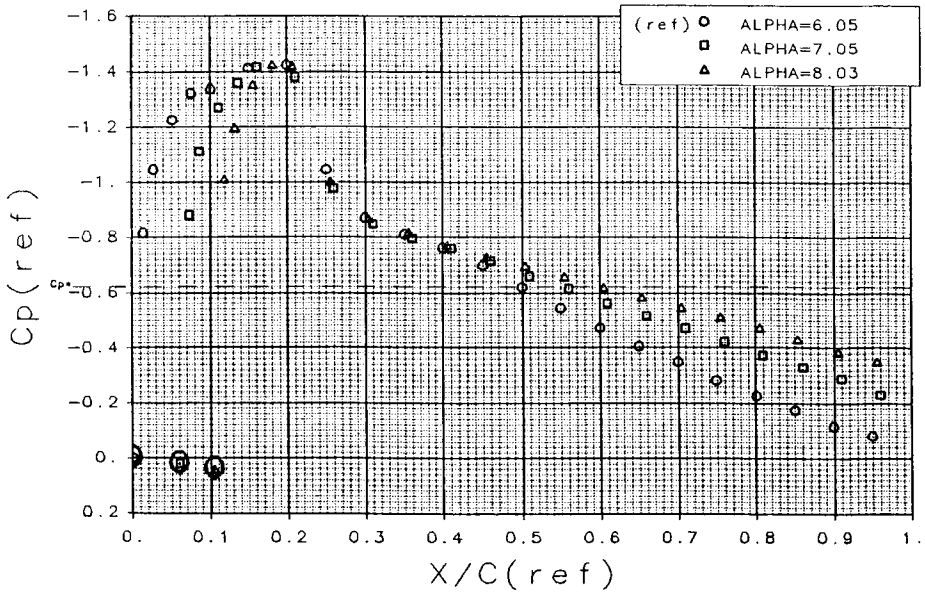

Figure A-4 NACA 0012 Airfoil, M=0.74, R_e=9x10^6

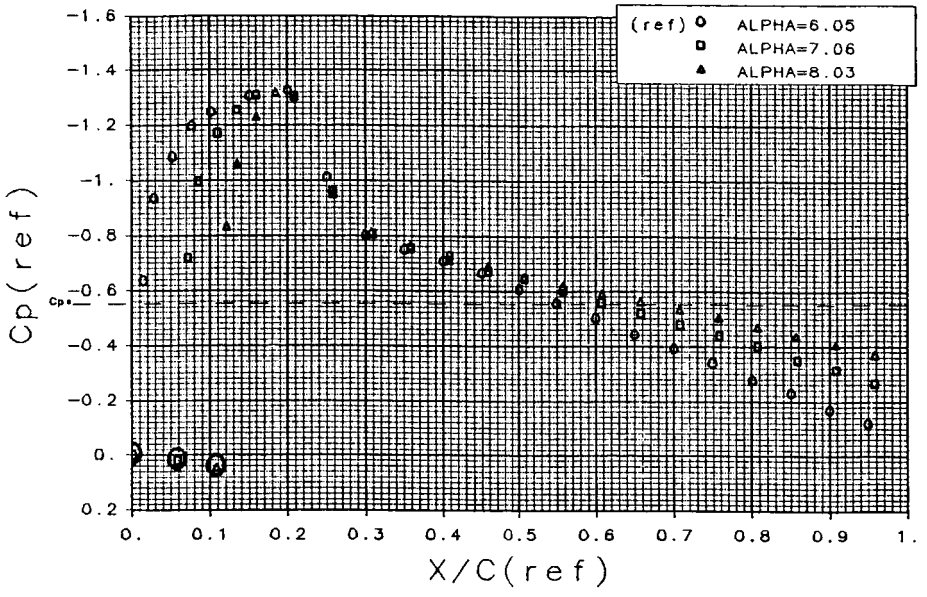

Figure A-5 NACA 0012 Airfoil, M=0.76, R_e=15x10^6

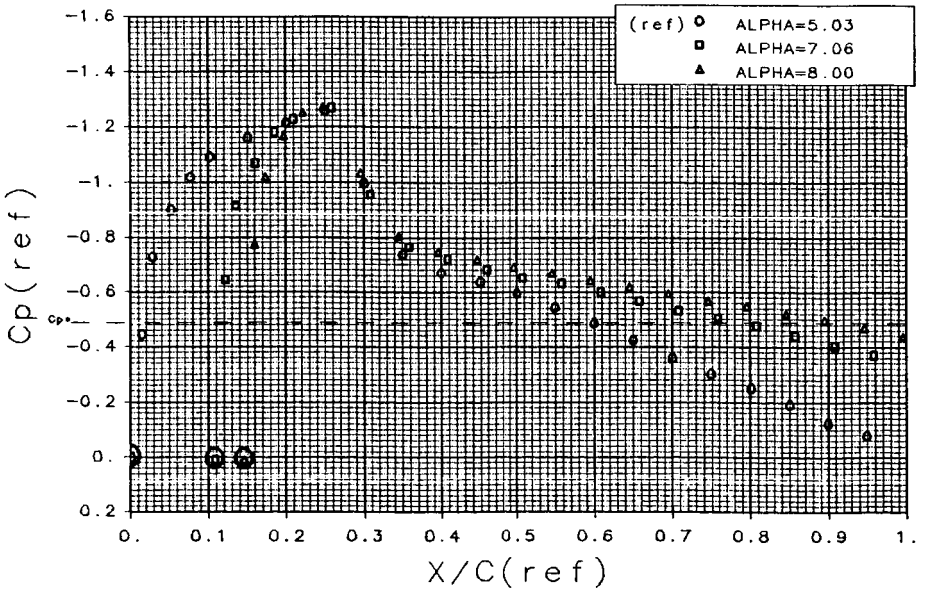

Figure A-6 NACA 0012 Airfoil, M=0.78, R_e=15x10^6

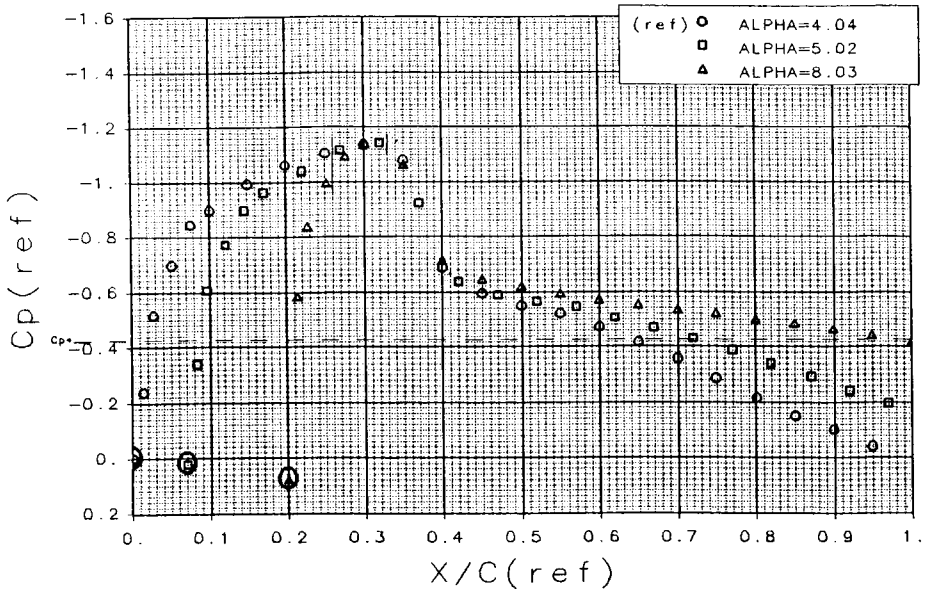

Figure A-7 NACA 0012 Airfoil, M=0.80, R_e=15x10^6

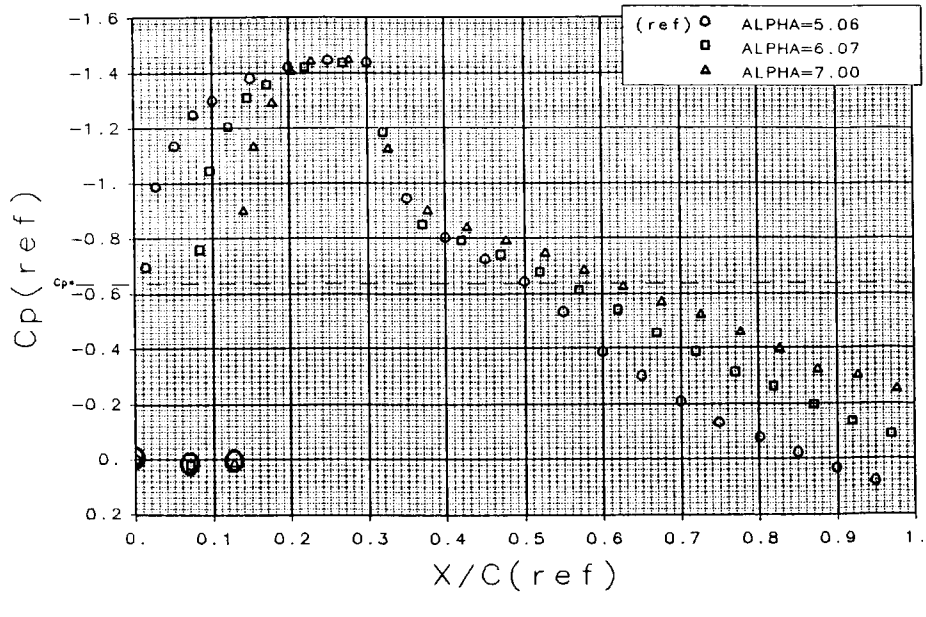

Figure A-8 NACA 0012 Airfoil, M=0.74, R_e=30x10^6

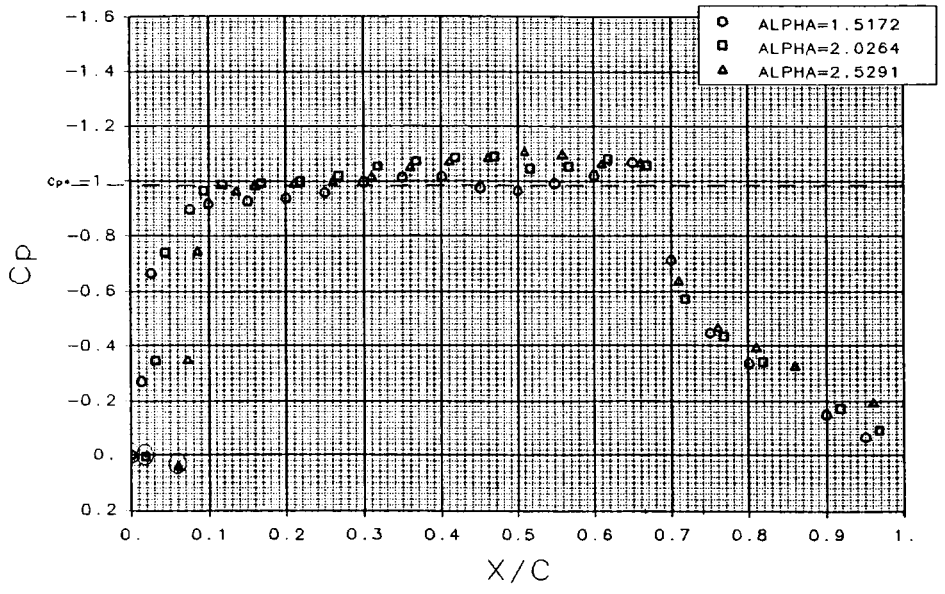

Figure A-9 SC(3)-0712(b) Airfoil, M=0.78, R_e=10x10^6

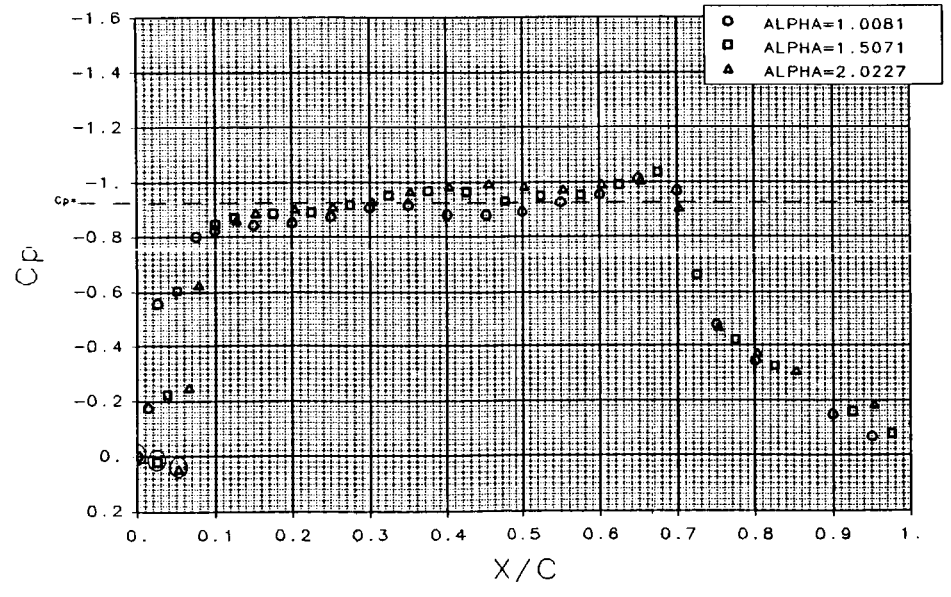

Figure A-10 SC(3)-0712(b) Airfoil, M=0.79, R_e=10x10^6

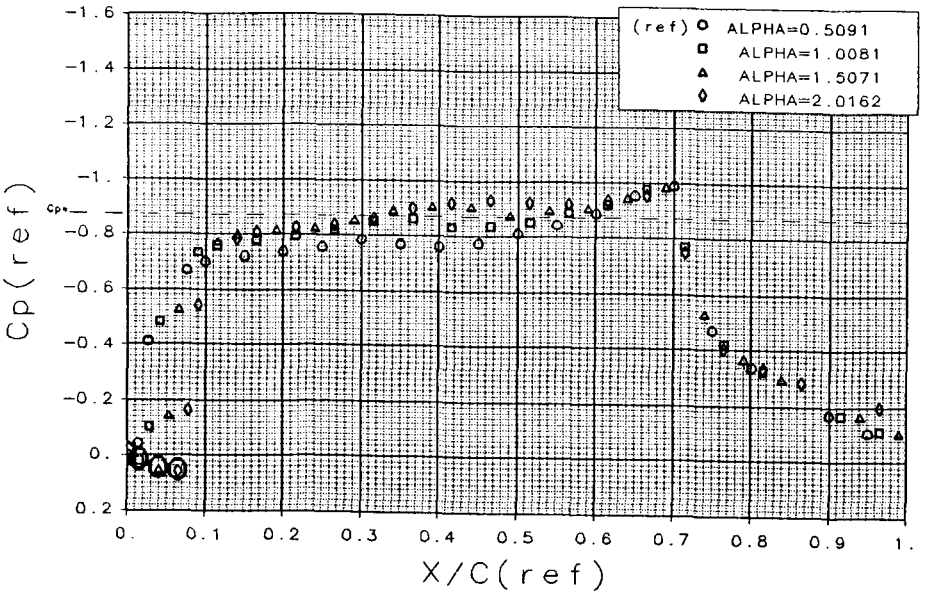

Figure A-11 SC(3)=0712(b) Airfoil, M=0.80, R_e=10x10^6

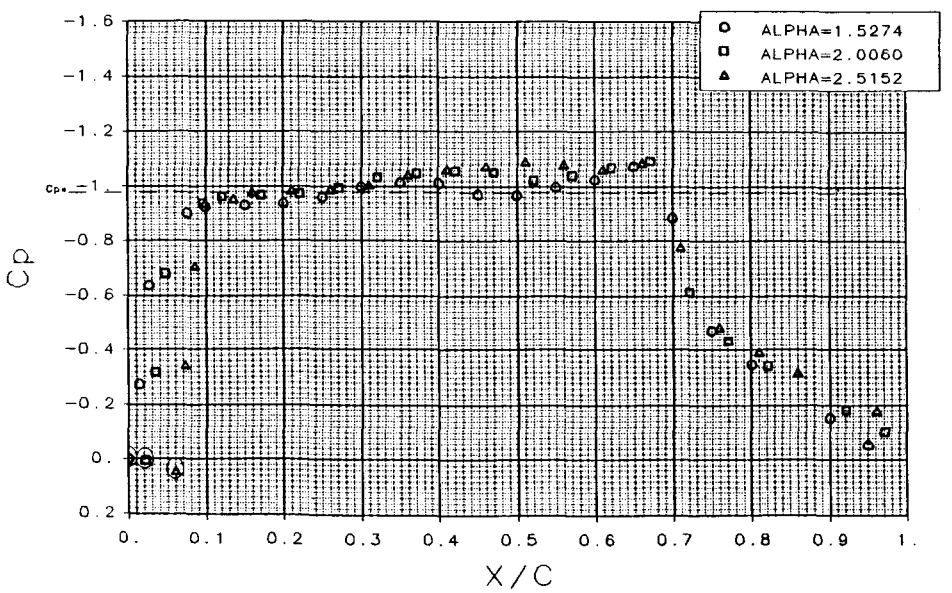

Figure A-12 SC(3)-0712(b) Airfoil, M=0.78, R_e=15x10^6

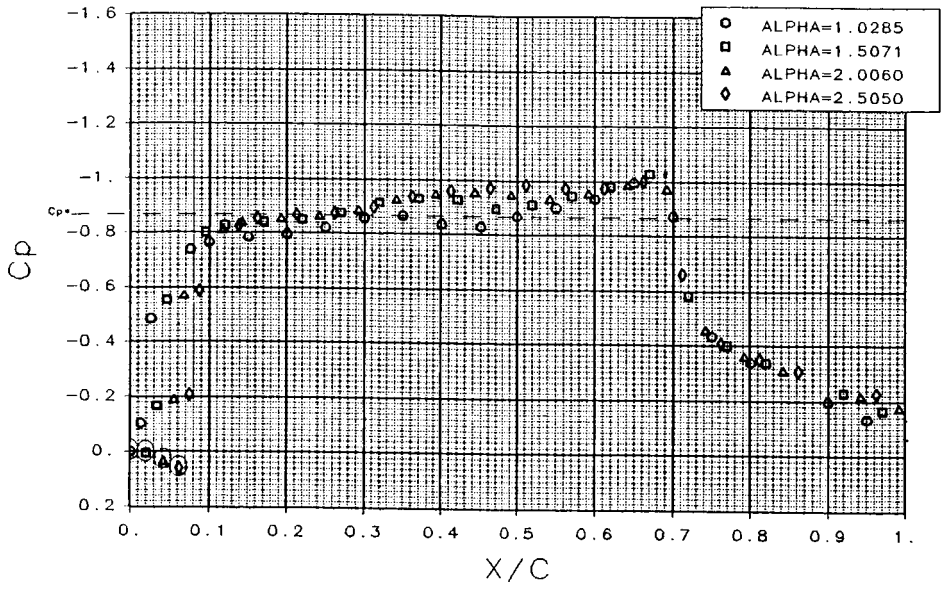

Figure A-13 SC(3)-0712(b) Airfoil, M=0.80, R_e=15x10^6

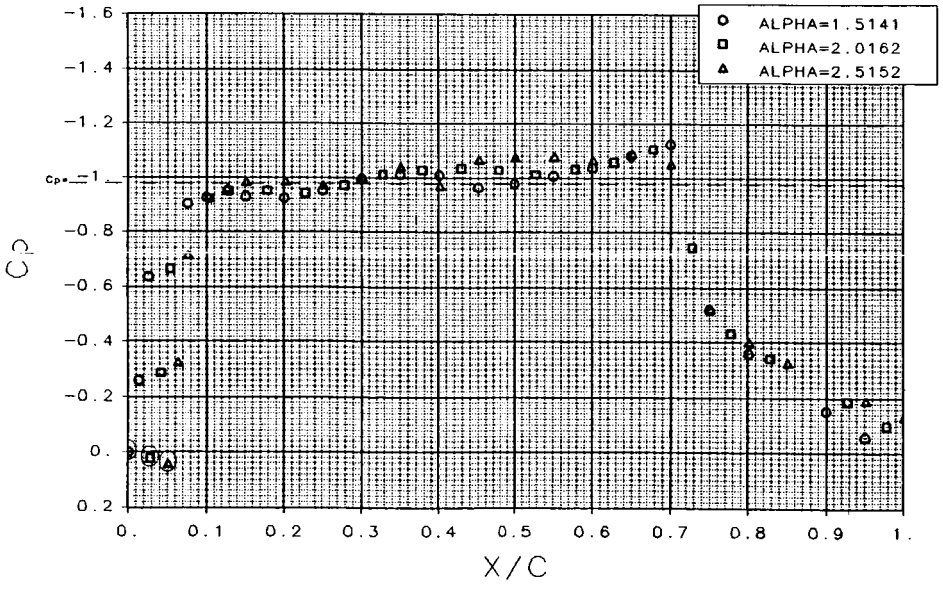

Figure A-14 SC(3)-0712(b) Airfoil, M=0.78, R_e=30x10^6

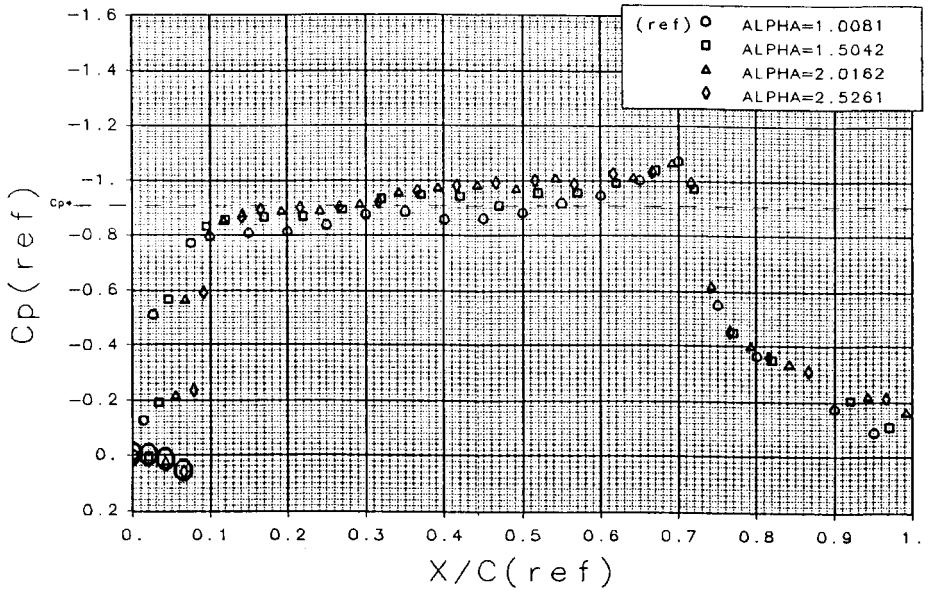

Figure A-15 SC(3)-0712(b) Airfoil, M=0.79, R_e=30x10^6

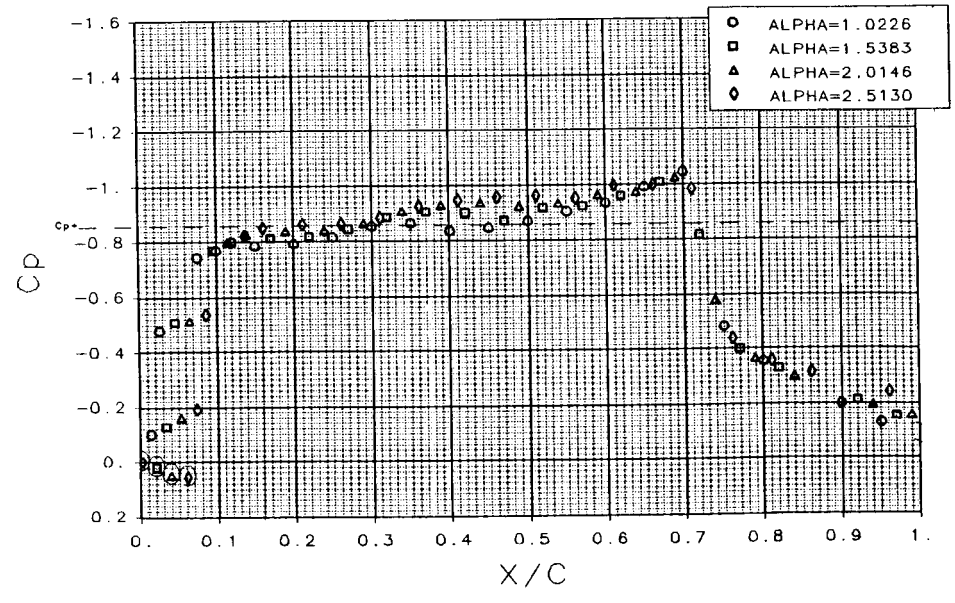

Figure A-16 SC(3)-0712(b) Airfoil, M=0.80, R_e=30x10^6

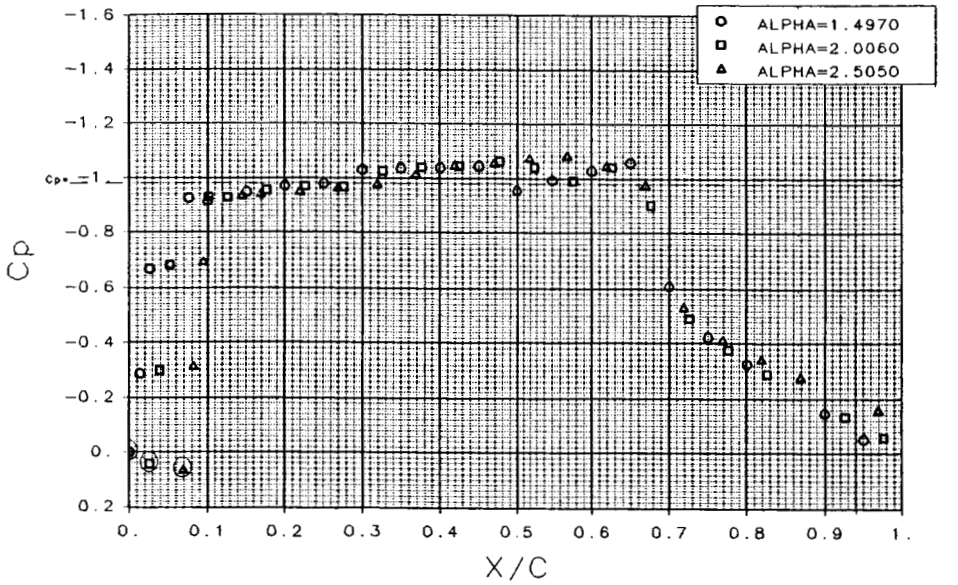

Figure A-17 SC(3)-0712(b) Airfoil, M=0.78, R_e=10x10^6 (Fixed Transition)

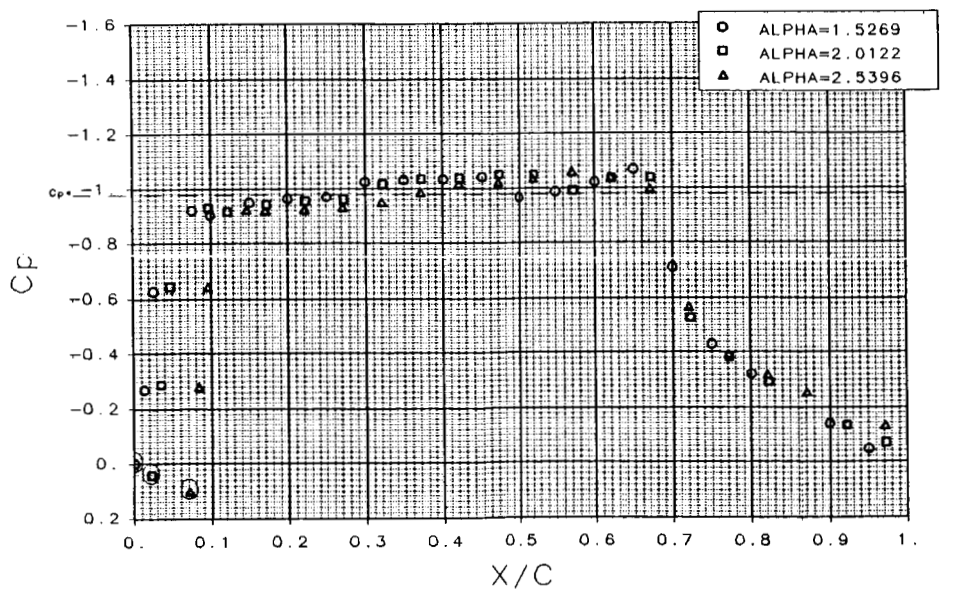

Figure A-18 SC(3)-0712(b) Airfoil, M=0.78, R_e=15x10^6 (Fixed Transition)

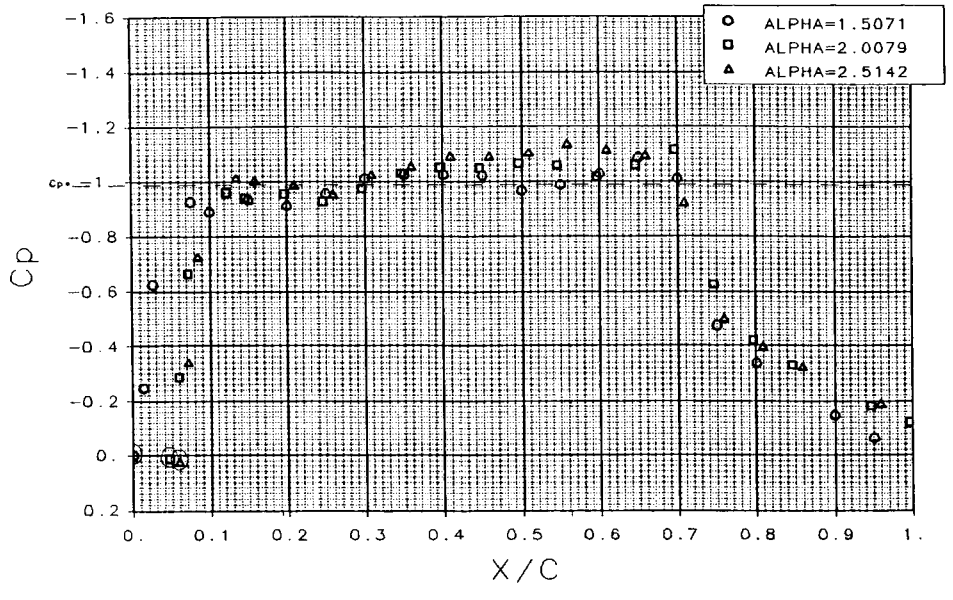

Figure A-19 SC(3)-0712(b) Airfoil, M=0.78, R_e=30x10^6 (Fixed Transition)

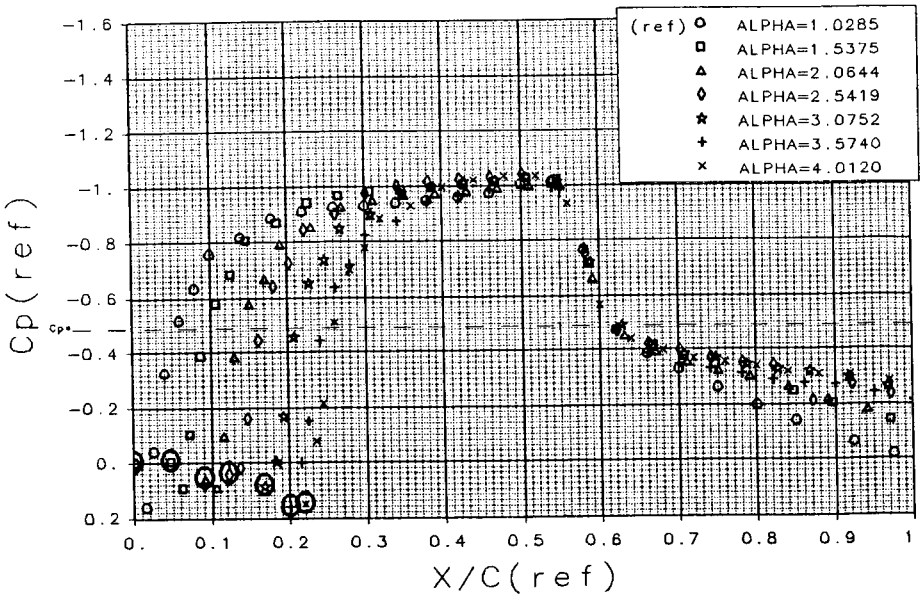

Figure A-20 CAST 10-2/DOA Airfoil, M=0.78, R_e=4x10^6

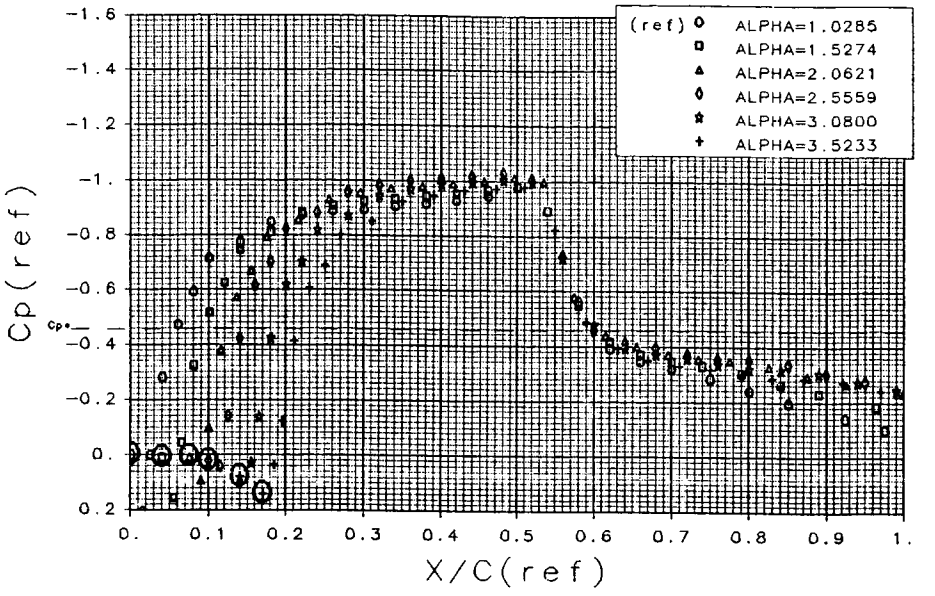

Figure A-21 CAST 10-2/DOA Airfoil, M=0.79, R_e=4x10^6

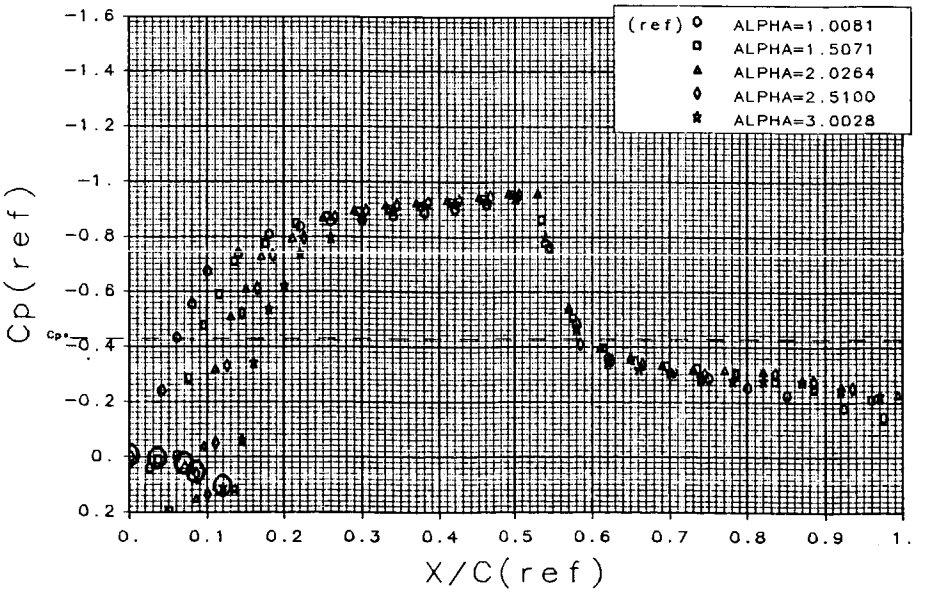

Figure A-22 CAST 10-2/DOA Airfoil, M=0.80, R_e=4x10^6

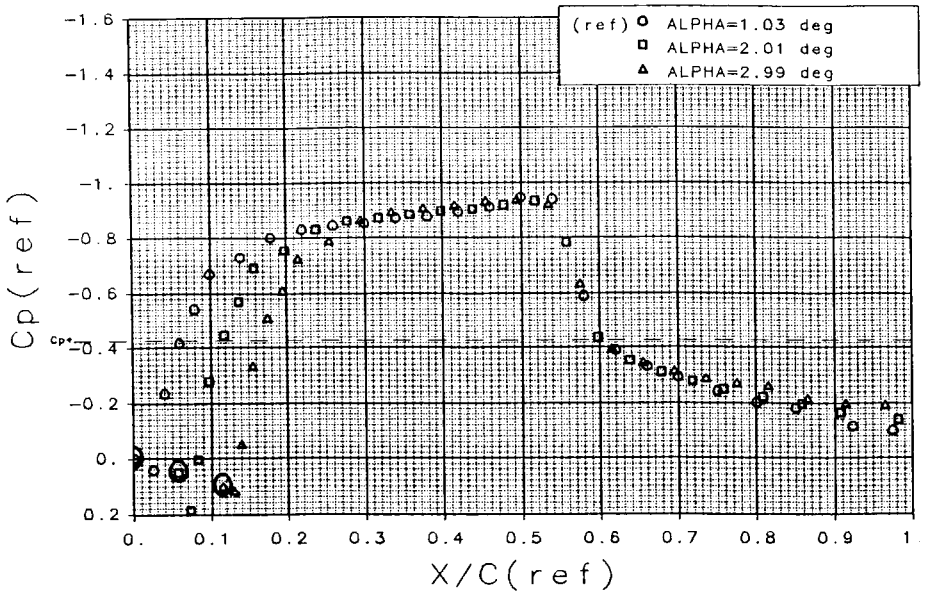

Figure A-23 CAST 10-2/DOA Airfoil, M=0.80, R_e=6x10^6

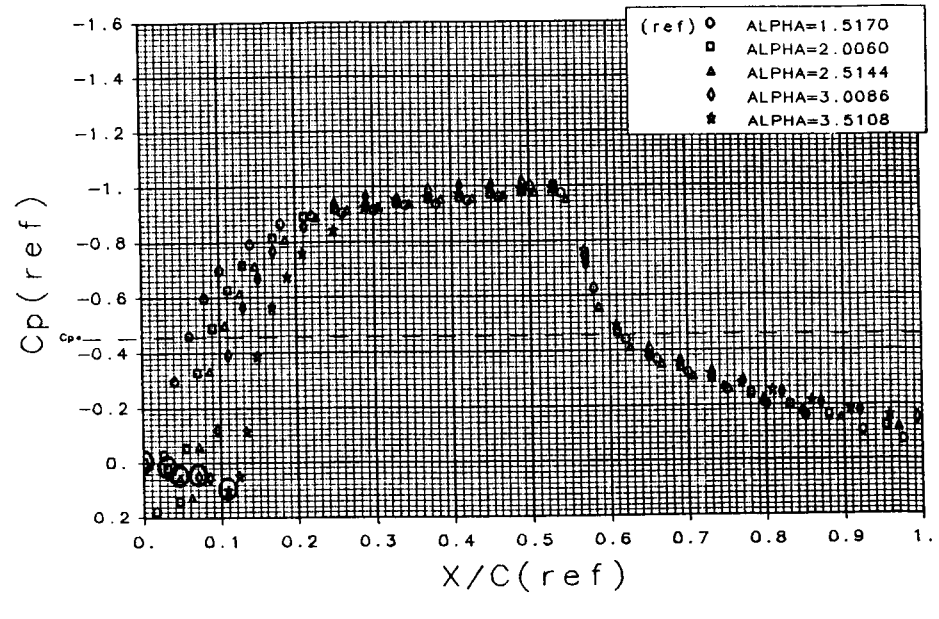

Figure A-24 CAST 10-2/DOA Airfoil, M=0.79, R_e=10x10^6

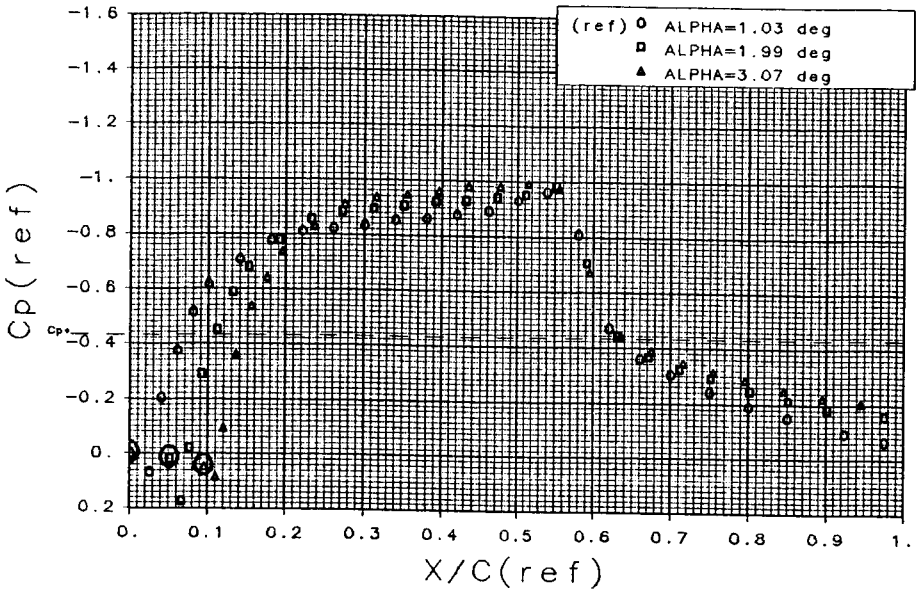

Figure A-25 CAST 10-2/DOA Airfoil, M=0.80, R_e=10x10^6

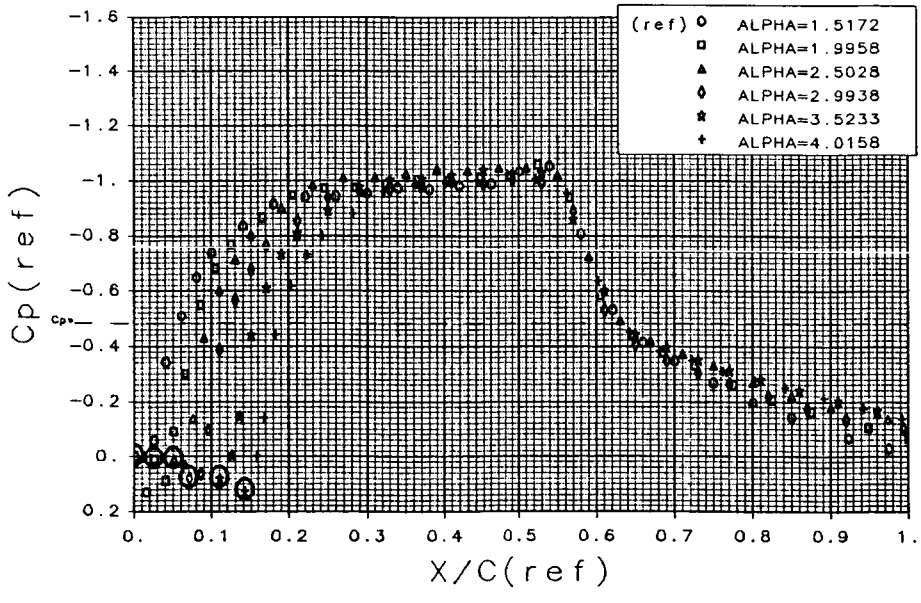

Figure A-26 CAST 10-2/DOA Airfoil, M=0.78, R_e=15x10^6

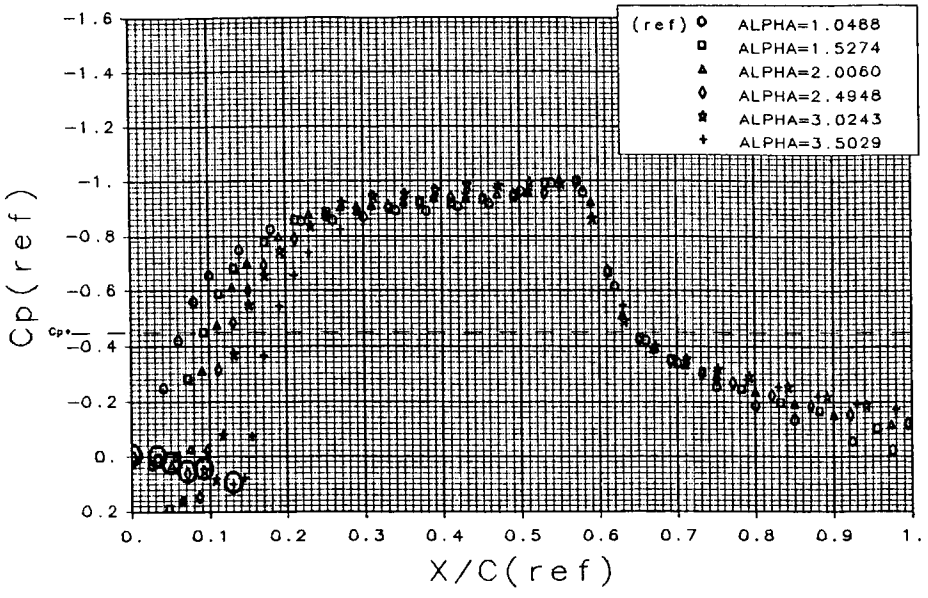

Figure A-27 CAST 10-2/DOA Airfoil, M=0.79, R_e=15x10^6

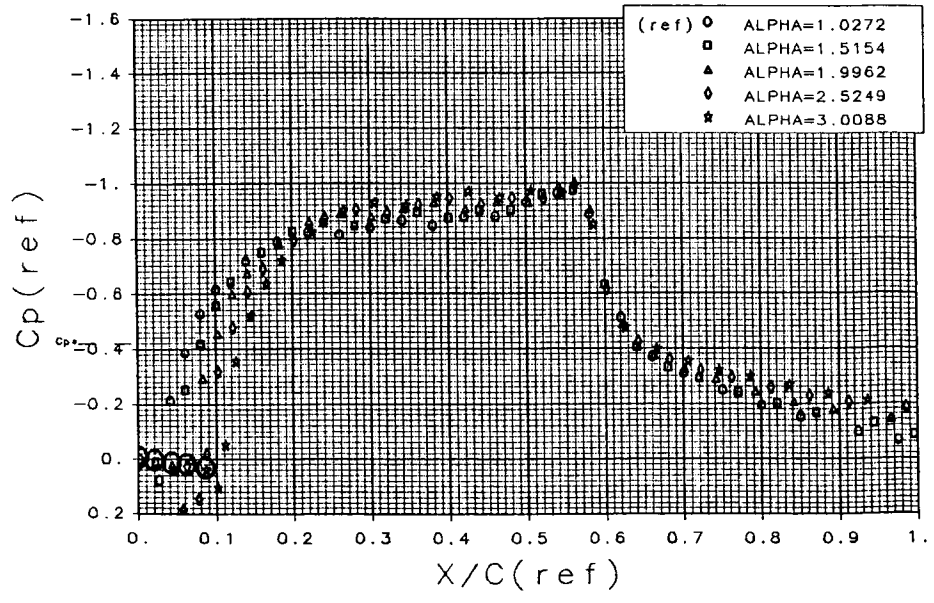

Figure A-28 CAST 10-2/DOA Airfoil, M=0.80, R_e=15x10^6

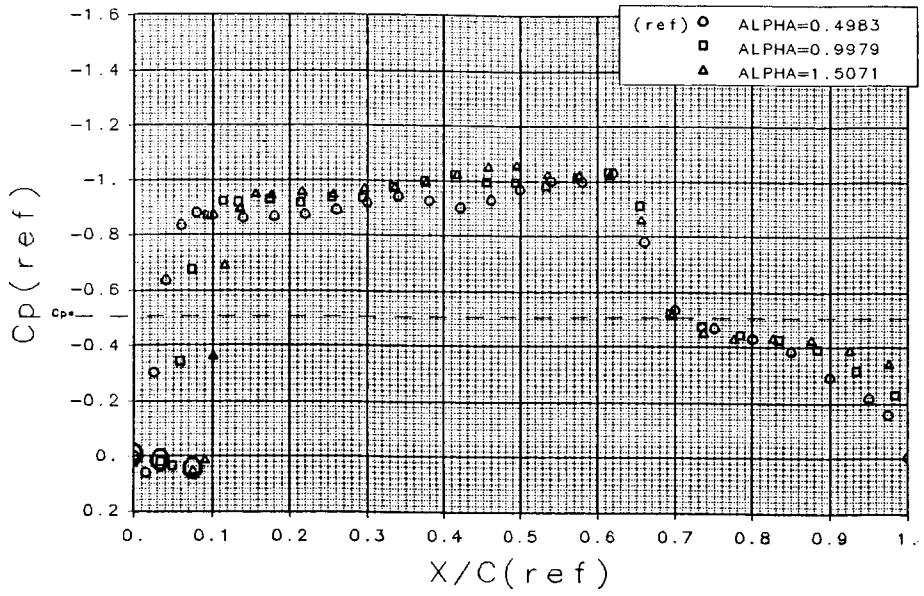

Figure A-29 DFVLR R4 Airfoil, M=0.78, R_e=4x10^6

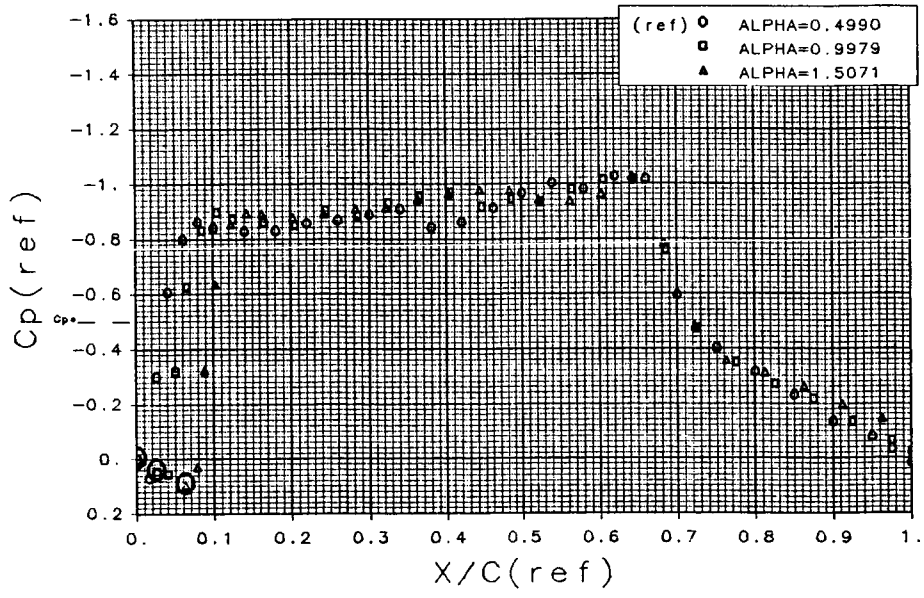

Figure A-30 DFVLR R4 Airfoil, M=0.78, R_e=15x10^6

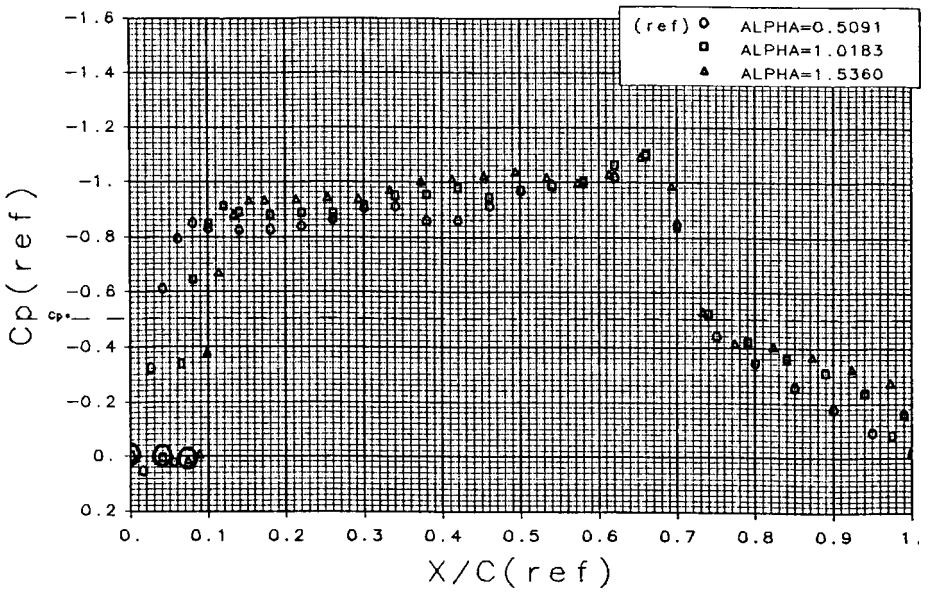

Figure A-31 DFVLR R4 Airfoil, M=0.78, R_e=40x10^6

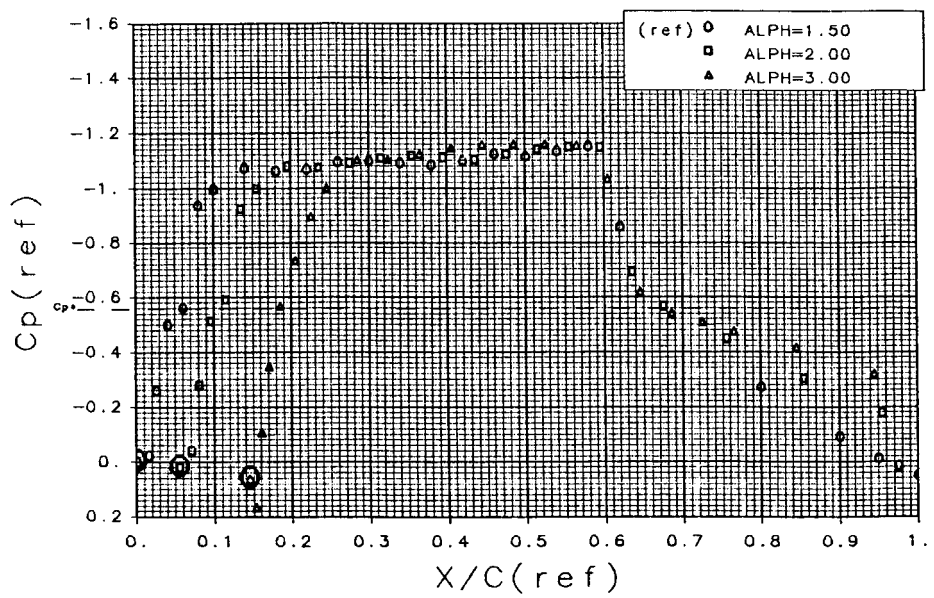

Figure A-32 CAST 7 Airfoil, M=0.76, R_e=6x10^6

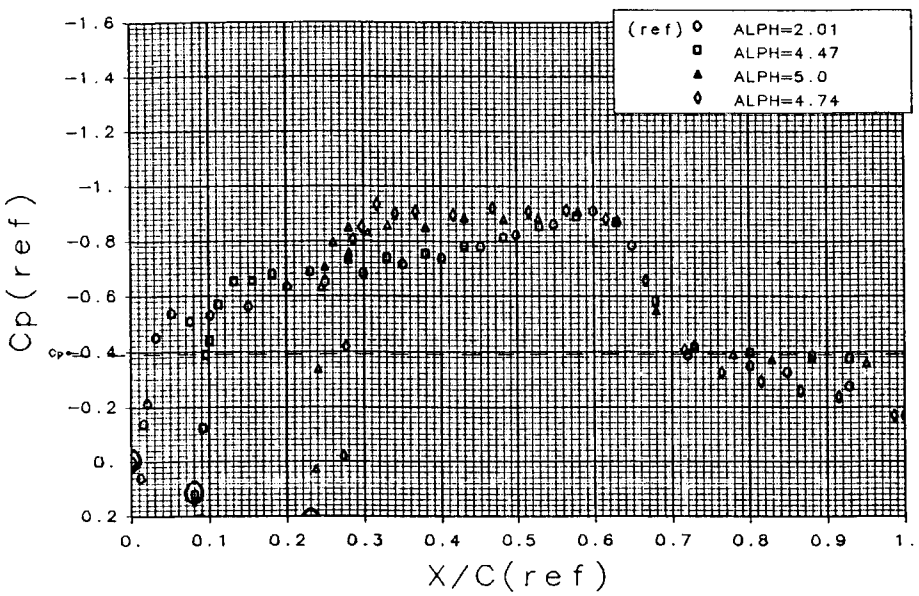

Figure A-33 MBB-A3 Supercritical Airfoil, M=0.80, R_e=6x10^6

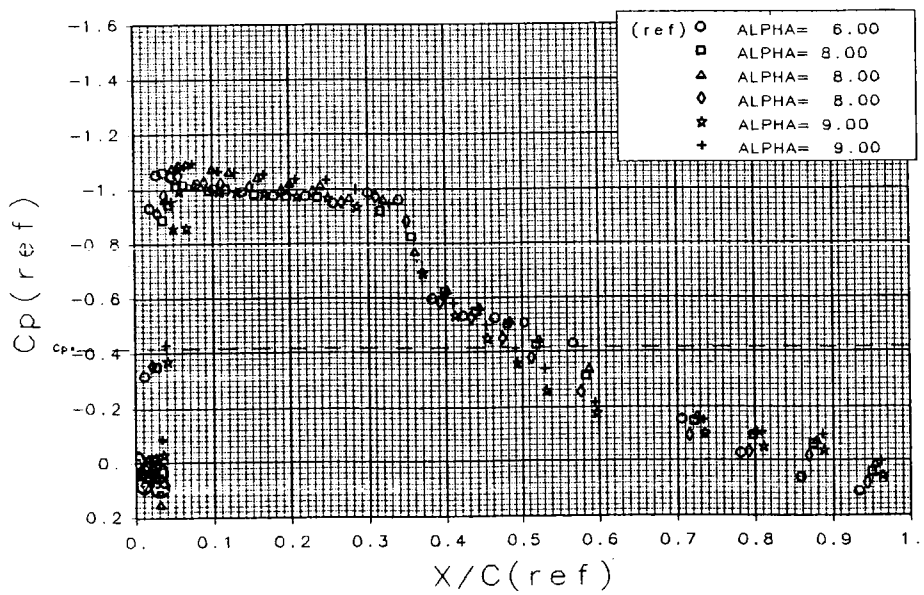

Figure A-34 ONERA D Airfoil, M=0.81, R_e=4.5x10^6

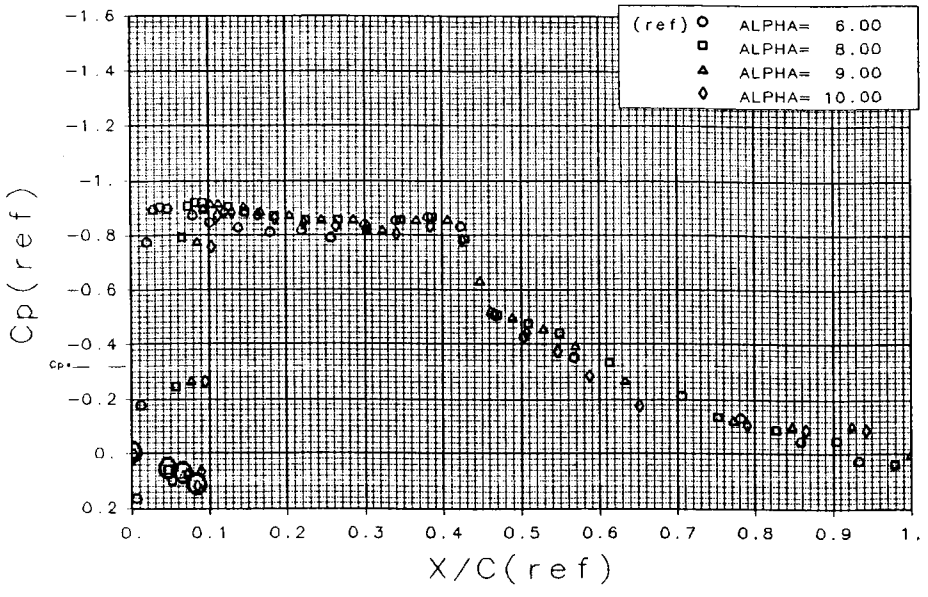

Figure A-35 ONERA D Airfoil, M=0.84, R_e=4.5x10^6

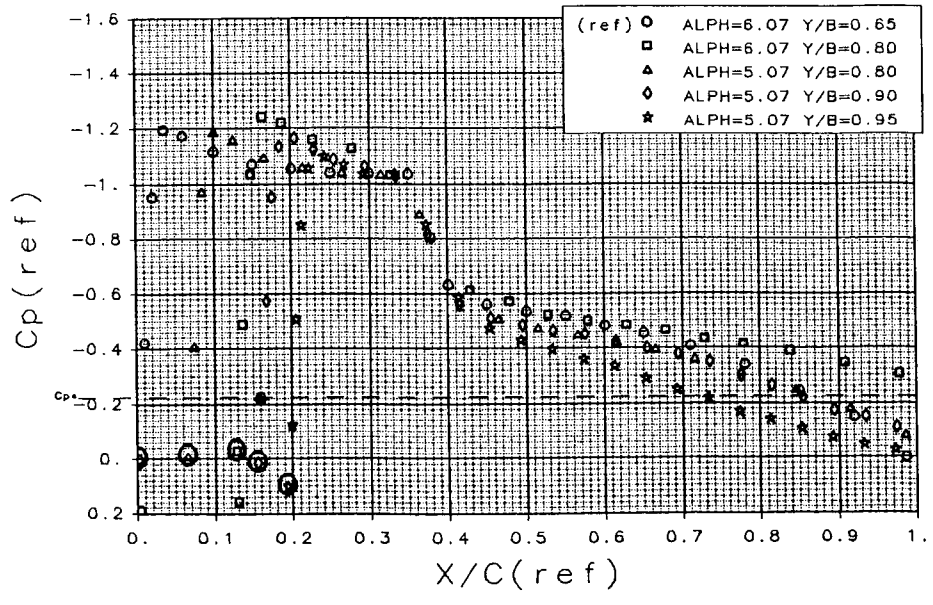

Figure A-36 ONERA M-6 Wing, M=0.88, R_e=12x10^6

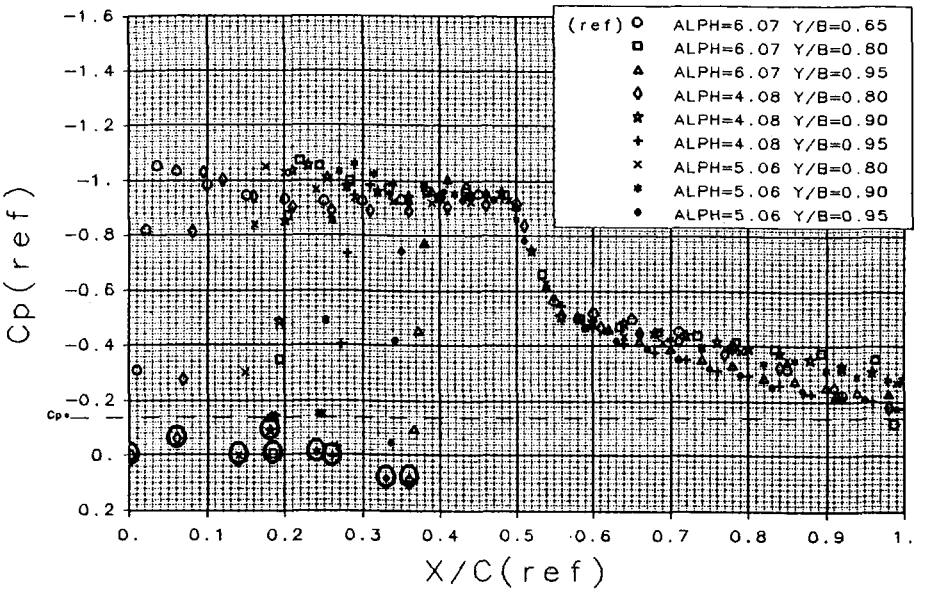

Figure A-37 ONERA M-6 Wing, M=0.93, R_e=12x10^6

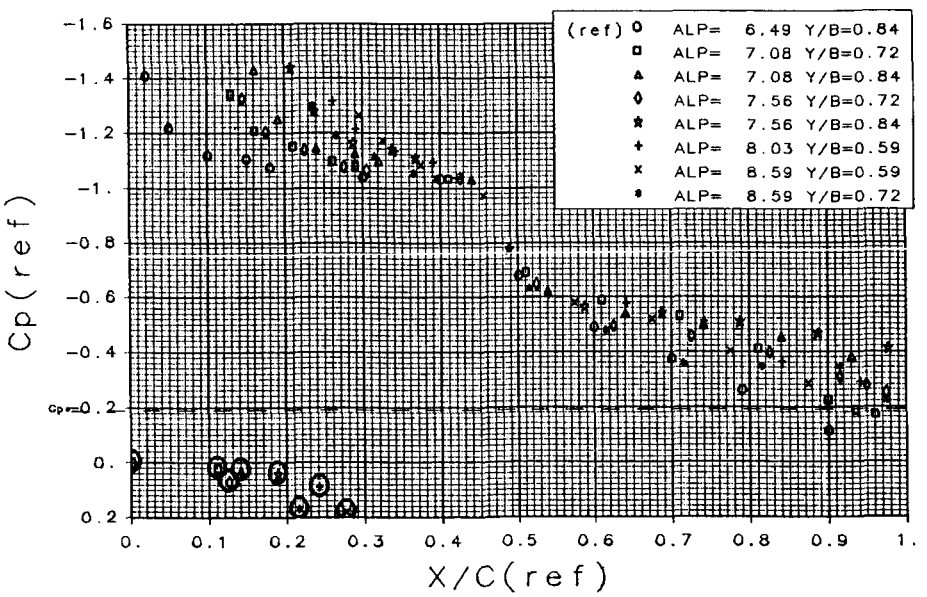

Figure A-38 F-16 1/9-Scale Model, M=0.90, R_e=2.5x10^6

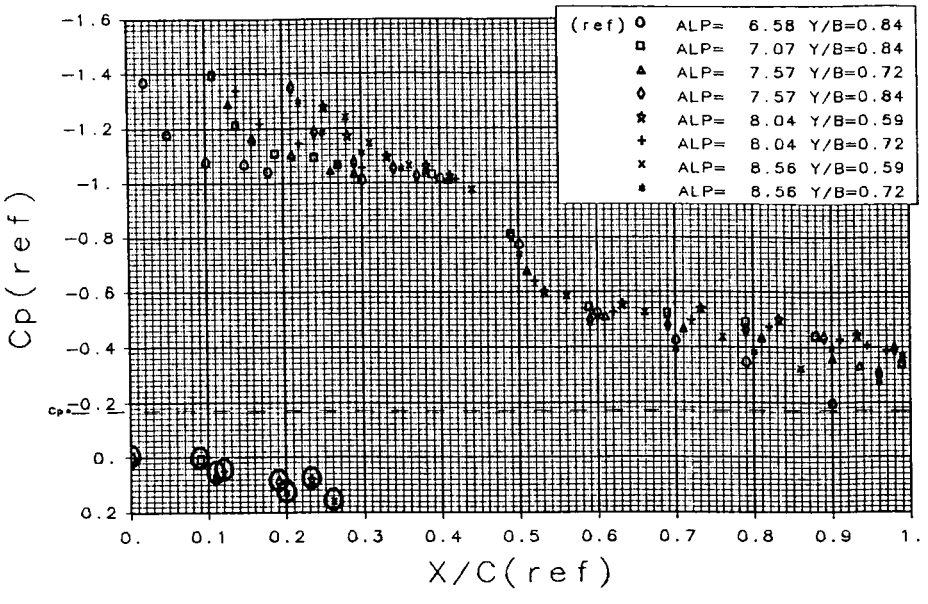

Figure A-39 F-16 1/9-Scale Model, M=0.91, R_e=2.5x10^6

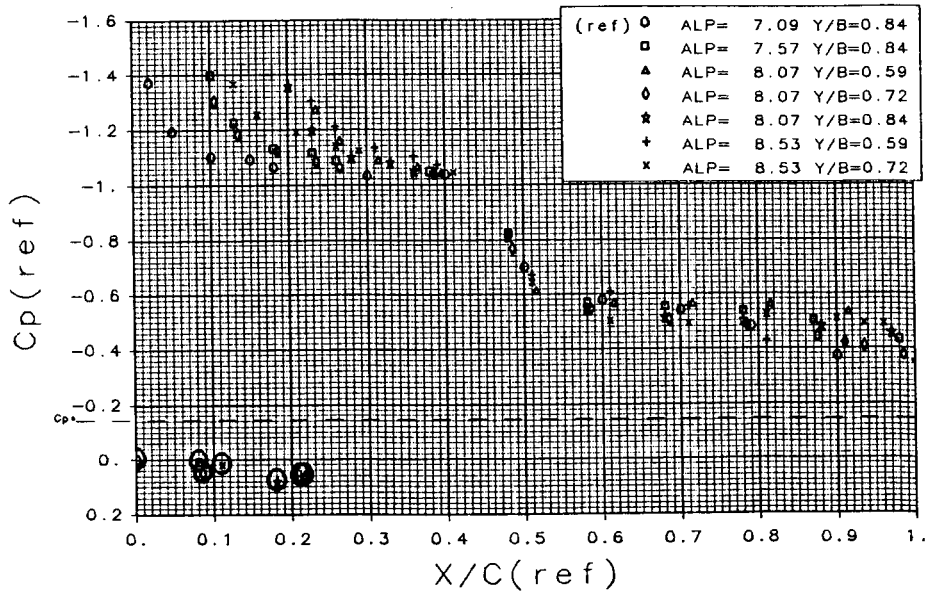

Figure A-40 F-16 1/9-Scale Model, M=0.92, R_e=2,5x10^6

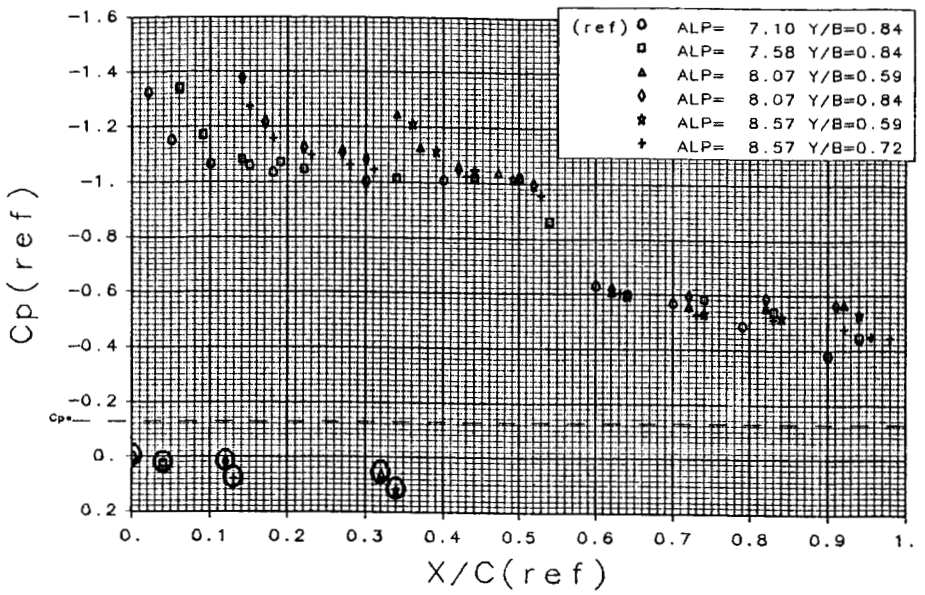

Figure A-41 F-16 1/9-Scale Model, M=0.93, R_e=2.5x10^6

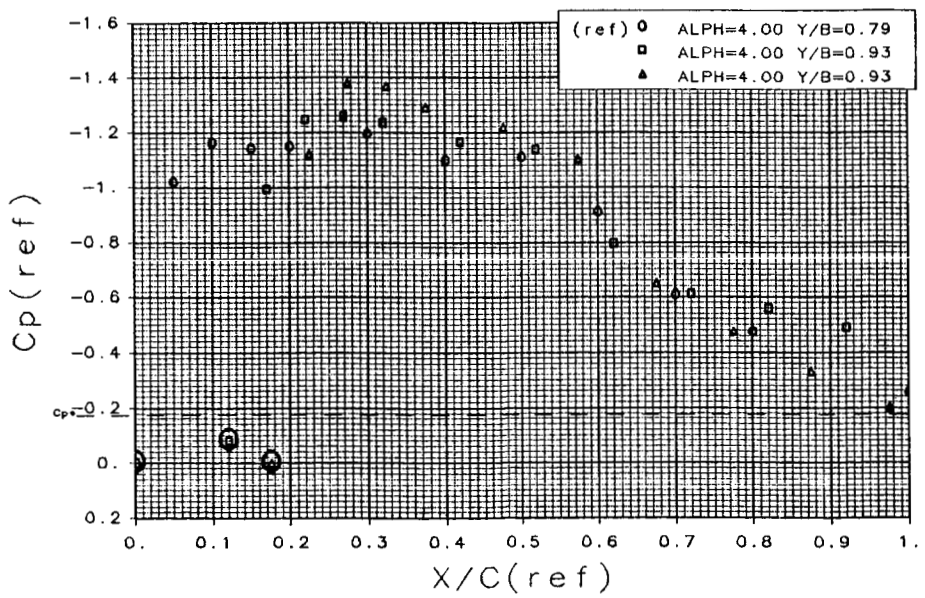

Figure A-42 MBB Wing/Body, M=0.90, R_e=1.34x10^6

Standard Bibliographic Page

1. Report No.	2. Government Accession No.	3. Recipient's Catalog No.
NASA CR-4090		

4. Title and Subtitle	5. Report Date
A Study of the Effects of Reynolds Number and Mach Number on Constant Pressure Coefficient Jump for Shock-Induced Trailing-Edge Separation	August 1987
	6. Performing Organization Code
7. Author(s)	8. Performing Organization Report No.
Atlee M. Cunningham, Jr., and Gregory S. Spragle	
9. Performing Organization Name and Address	10. Work Unit No.
General Dynamics Corporation P.O. Box 748 Fort Worth, Texas 76101	505-60-21-01
	11. Contract or Grant No.
	NAS1-17955
12. Sponsoring Agency Name and Address	13. Type of Report and Period Covered
National Aeronautics and Space Administration Washington, D.C. 20546	Contractor Report
	14. Sponsoring Agency Code

15. Supplementary Notes

Langley Technical Monitor: Elizabeth B. Plentovich

Final Report

16. Abstract

A study was conducted to address the influence of Mach and Reynolds numbers as well as airfoil and planform geometry on the phenomenon of constant shock jump pressure coefficient for conditions of shock-induced trailing-edge separation (SITES). It was demonstrated that the phenomenon does exist for a wide variety of two- and three-dimensional flow cases and that the influence of free stream Mach number was not significant. The influence of Reynolds number was found to be important but was not strong. Airfoil and planform geometric characteristics were found to be very important where the C_p jump was shown to vary with the sum of (1) airfoil curvature at the upper surface crest and (2) camber surface slope at the trailing edge. It was also determined that the onset of SITES could be defined as a function of airfoil geometric parameters and Mach number normal to the leading edge. This onset prediction was shown to predict the angle of onset to within $\pm 1^{\circ}$ accuracy or better for about 90% of the cases studied.

17. Key Words (Suggested by Authors(s))	18. Distribution Statement
Aerodynamic Pressures Transonic Flow Shock-Induced Separation Trailing-Edge Pressure Divergence	Unclassified - Unlimited Subject Category 02

19. Security Classif.(of this report)	20. Security Classif.(of this page)	21. No. of Pages	22. Price
Unclassified	Unclassified	80	A05

For sale by the National Technical Information Service, Springfield, Virginia 22161